The prompt emission phase of gamma-ray bursts: recent results

Željka Bošnjak
University of Zagreb, Croatia

HEPRO Paris, October 23-26, 2023

Outline

I - GRB prompt emission from the synchrotron radiation of relativistic electrons and the low energy spectral slope

II - Off-axis MeV and very-high energy gamma-ray emissions from structured gamma-ray burst jets

I - GRB prompt emission from the synchrotron radiation of relativistic electrons in a decaying magnetic field

▸ Motivation

The theoretically predicted synchrotron spectrum leads to a slope $F_\nu \propto \nu^{-1/2}$ below 100 keV, which is in contradiction to the much harder spectra observed during the prompt GRB emission.

Sari, Piran & Narayan 1998

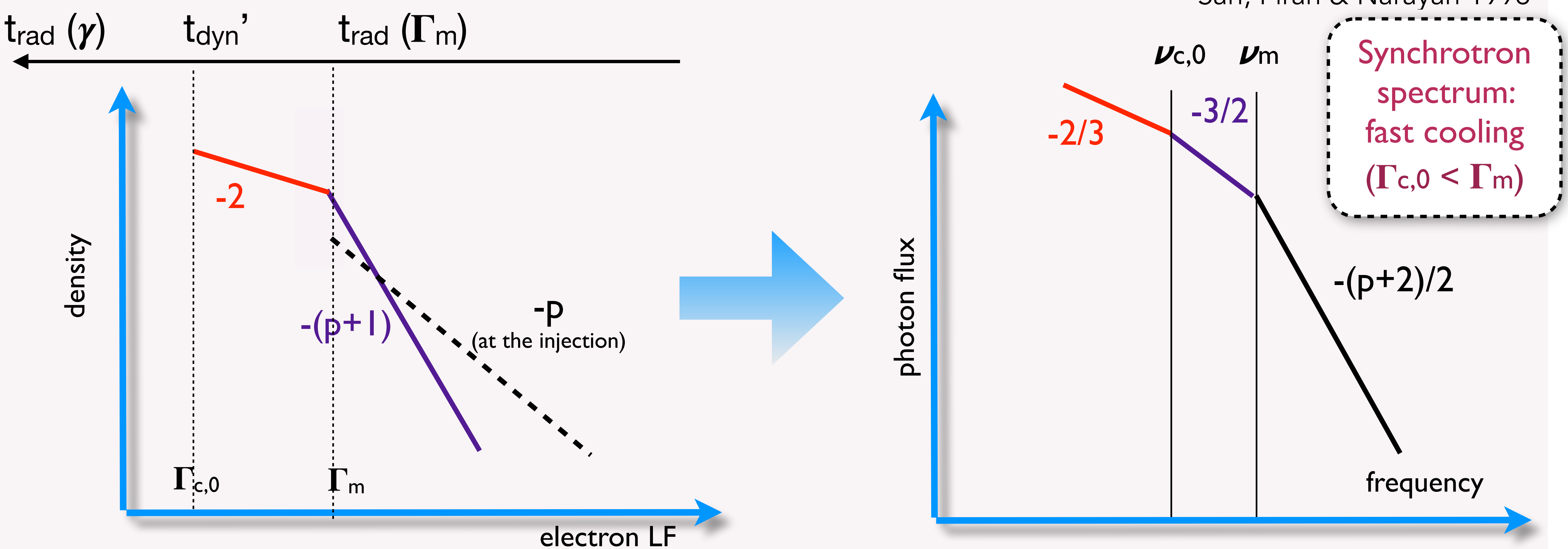

Γ_m: minimum Lorentz factor at injection

$\Gamma_{c,0}$: radiative timescale = dynamical timescale

A possible solution proposed by Daigne et al. 2011; Beniamini & Piran 2013: in **the marginally fast cooling regime** ($\Gamma_{c,0} \simeq (0.1 - 1)\, \Gamma_m$), where the cooling break is very close to the peak frequency, the intermediate portion of the spectrum (slope = -3/2) disappears and the slope -2/3 is recovered (still with a high radiative efficiency)

I - GRB prompt emission from the synchrotron radiation of relativistic electrons in a decaying magnetic field

- **Motivation**

Marginally fast cooling can naturally emerge if electrons are radiating in a magnetic field decaying on a timescale t_B',

$$B'(t') = B_0' \, e^{-t'/t'_B} \quad \text{where} \quad t'_{syn}(\boldsymbol{\Gamma}_m) < t'_B < t'_{dyn}$$

→ electrons having $\boldsymbol{\gamma} \gtrsim \boldsymbol{\Gamma}_m$ will still experience a magnetic field B'_0 and the peak + high-enegy part of the synchrotron spectrum will not be affected

→ electrons with Lorentz factors $\boldsymbol{\Gamma}_{c,0} < \boldsymbol{\gamma} < \boldsymbol{\Gamma}_m$ will lose their energy more slowly than expected because they will encounter a lower magnetic field when they start to travel outside the initial acceleration site. The cooling break will increase to:

$$\nu_c \simeq \nu_{c,0} \, (t'_{dyn} / t'_B)^2$$

This allows to naturally tend towards the marginally fast cooling regime, even when $\boldsymbol{\Gamma}_{c,0} / \boldsymbol{\Gamma}_m << 1$. The radiative efficiency will remain high as long as $t'_{syn}(\boldsymbol{\Gamma}_m) << t'_B$ so the final condition becomes:

$$\boldsymbol{\Gamma}_{c,0} / \boldsymbol{\Gamma}_m \lesssim t'_B / t'_{dyn} \lesssim 1$$

I - GRB prompt emission from the synchrotron radiation of relativistic electrons in a decaying magnetic field

- **Model**

We investigate the impact of the evolution of B′ on the observed prompt GRB spectrum.

Radiative processes:

synchrotron radiation
inverse Compton scatterings
photon-photon annihilation
synchrotron self-absorption
adiabatic cooling

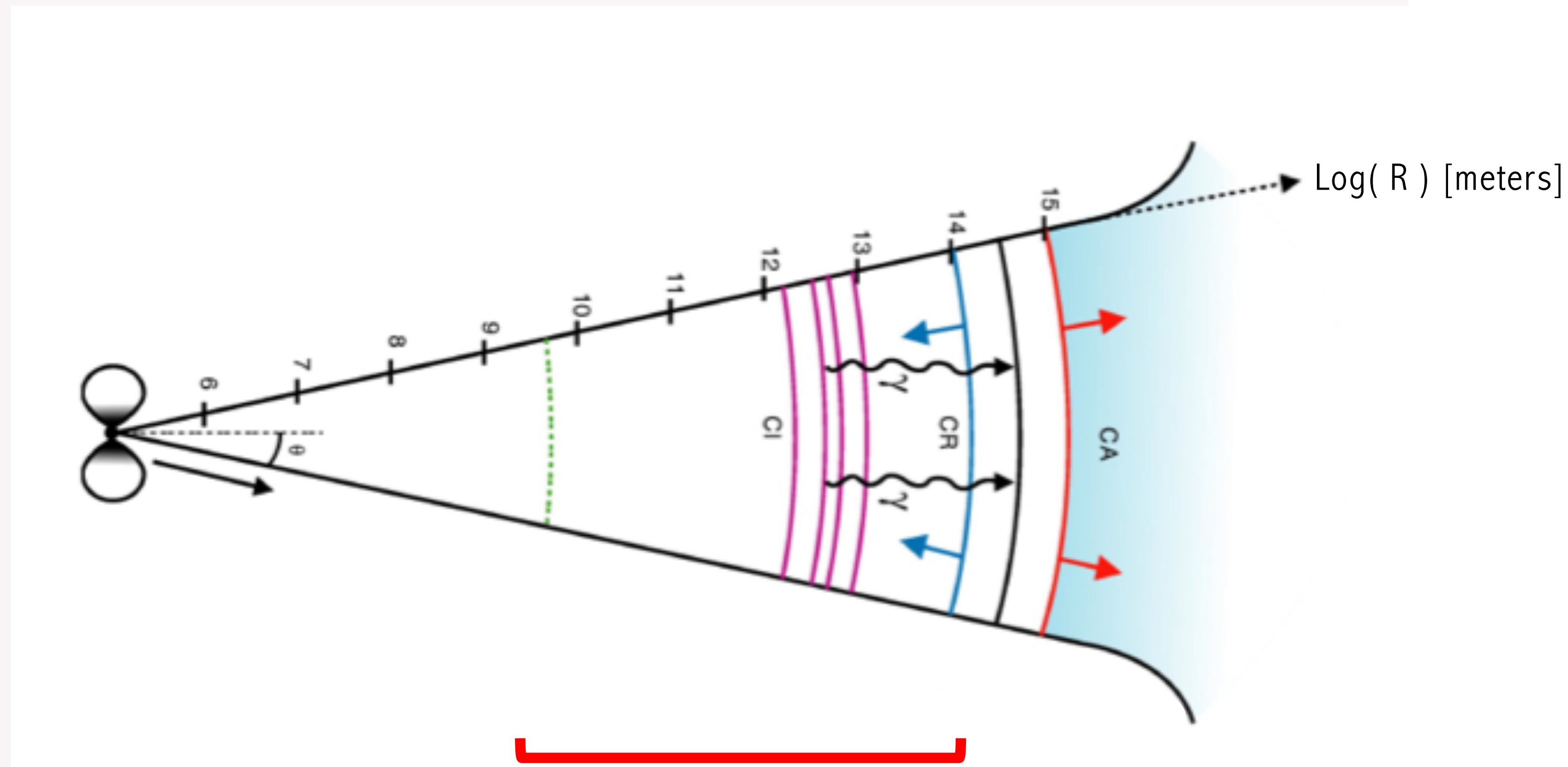

the region of the parameter space where the medium is optically thin for Thomson scatterings,

$\tau_T = \sigma_T\, n_e\, c\, t_{ex}' < 0.1$

- **Probing the parameter space**

Comoving frame parameters (B_0', t_{ex}', n_e, Γ_m)

Synchrotron spectrum

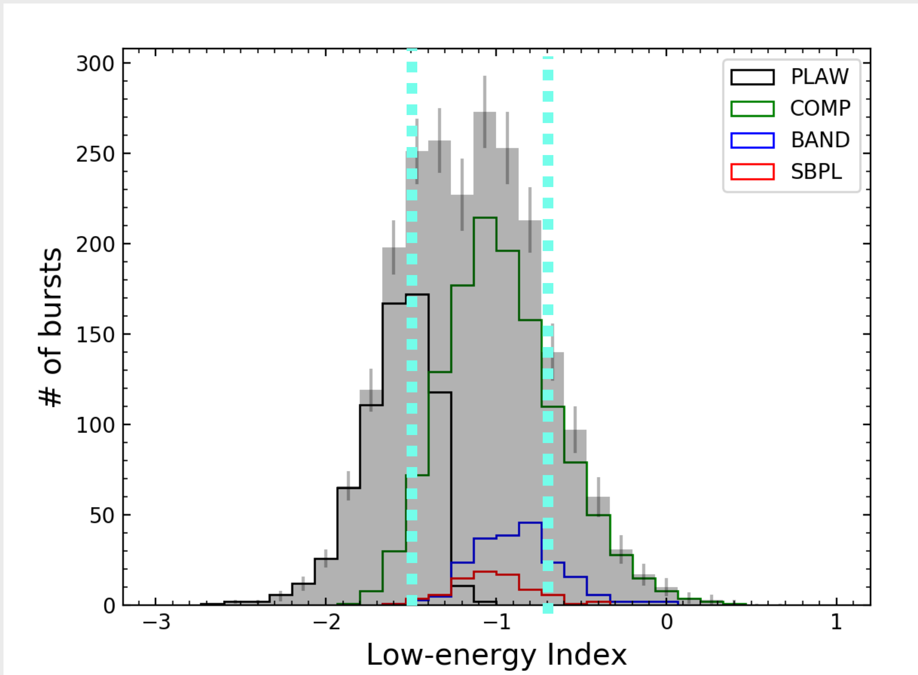

Time-integrated spectral fits: $\alpha = -1.08^{+0.45}_{-0.44}$

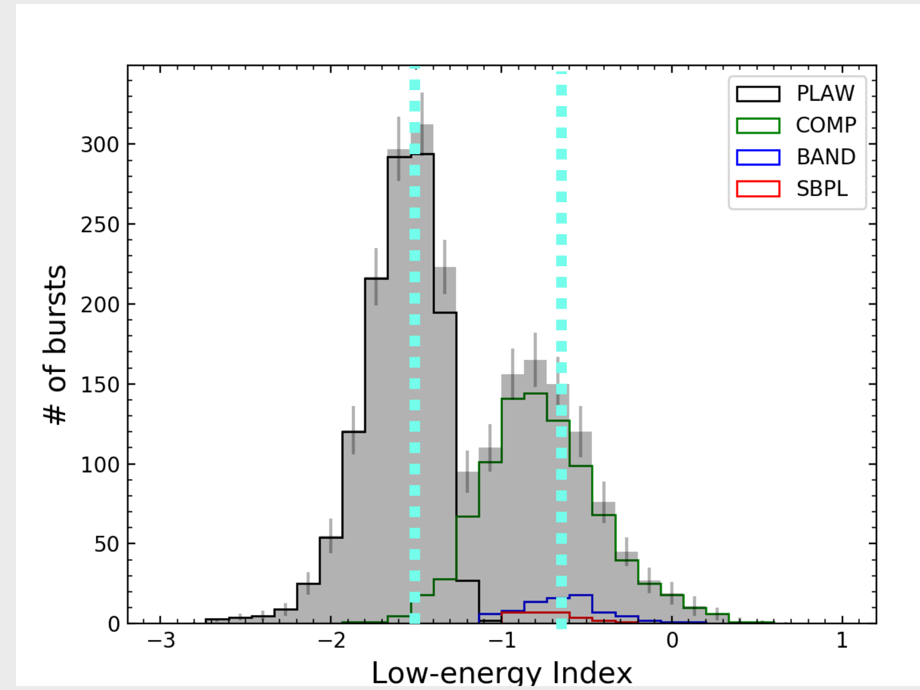

Peak-flux spectral fits: $\alpha = -1.30^{+0.77}_{-0.33}$

Poolakkil et al. 2021

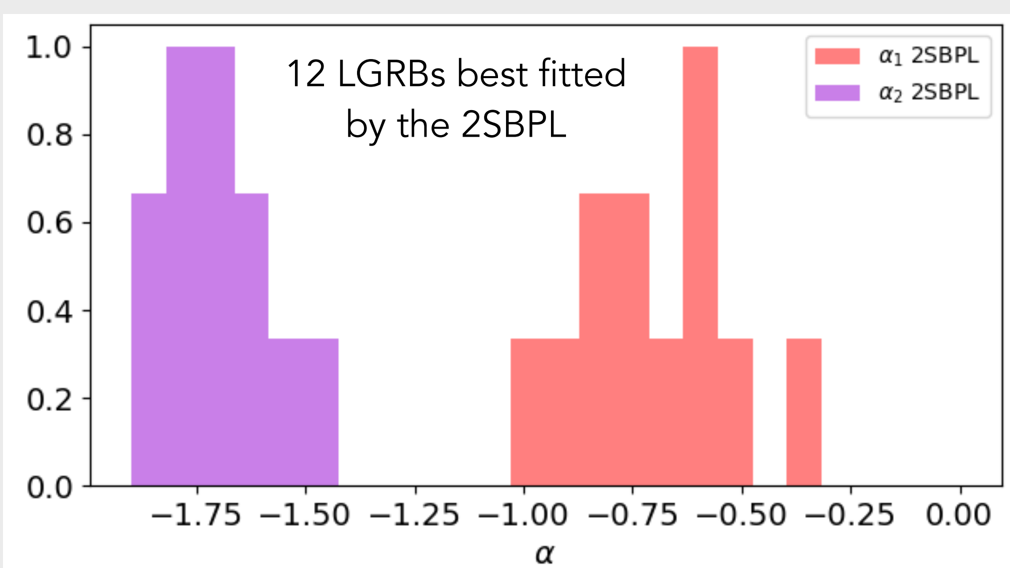

Toffano et al. 2021: 12 LGRBs observed by Fermi GBM, having large fluences and large E_{peak} values

→ the distributions of spectral slopes peak at -0.71 and -1.71, not far from the typical values -2/3 and -3/2 expected for synchrotron spectrum from marginally fast cooling electrons

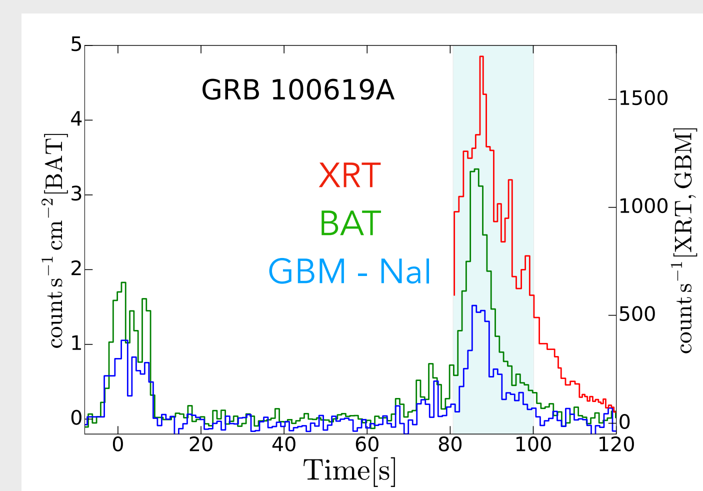

Oganesyan et al. 2018; 2017
joint XRT+BAT spectral analysis for 34 GRBs

Radiative models

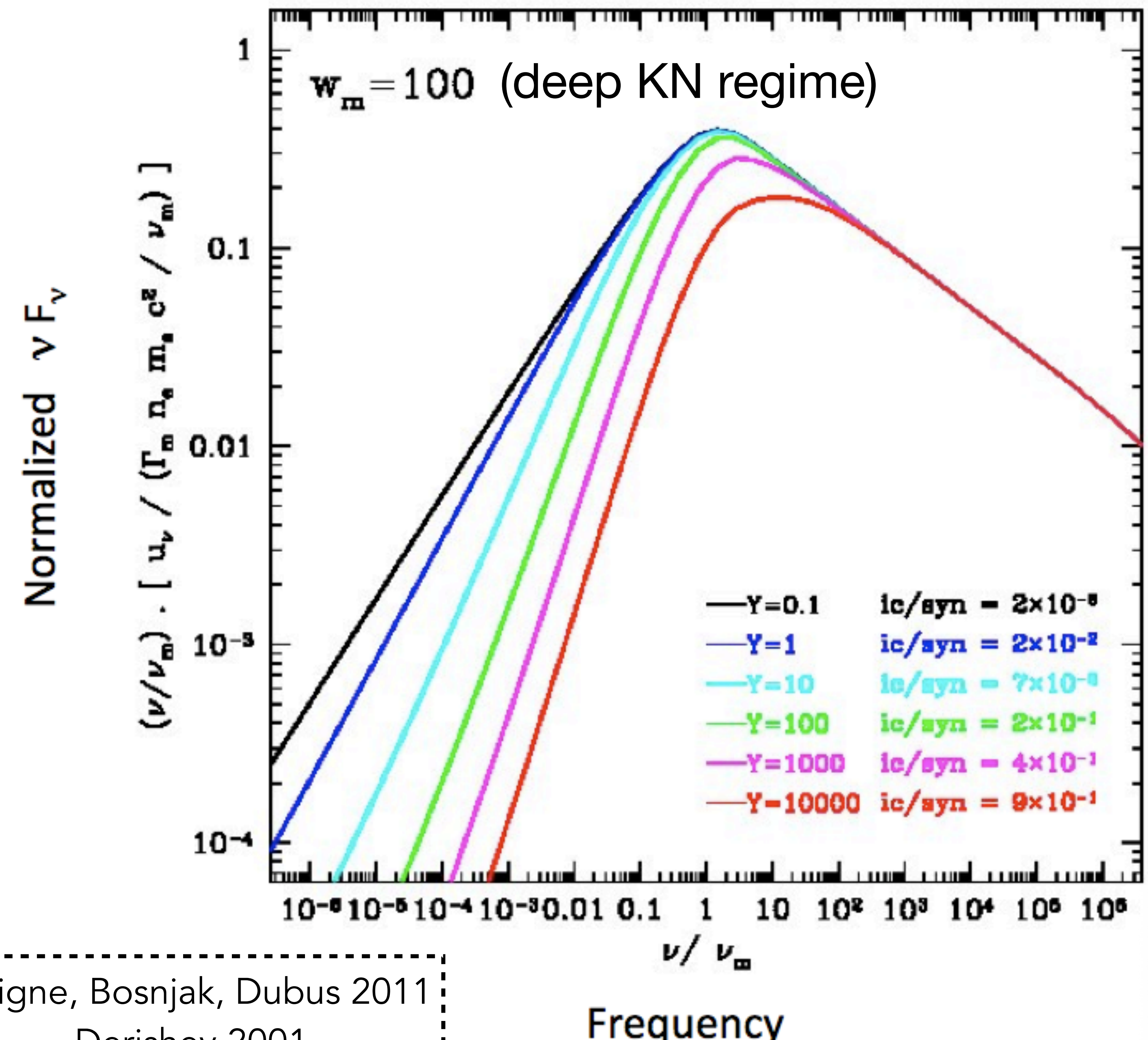

w_m : importance of KN

$$w_{\rm m} = \Gamma_{\rm m} \frac{h\nu'_{\rm m}}{m_{\rm e}c^2}$$

Y : importance of IC vs syn

$$Y = \frac{4}{3}\tau_{\rm T}\Gamma_{\rm m}\Gamma_{\rm c} \simeq \frac{\epsilon_{\rm e}}{\epsilon_{\rm B}}$$

Thomson regime: the electron cooling rate due to IC scatterings remains proportional to γ^2 as for the synchrotron power

KN regime: the electron cooling rate due to IC depends on γ

Daigne, Bosnjak, Dubus 2011
Derishev 2001
Nakar et al. 2009

Radiative models

Radiating electrons probe the magnetic field on >> scale than in the PIC simulations but - when they are in fast cooling - on a much smaller scale than the (magneto-) hydrodynamical scale.

A hierarchy of scales: $t'_{acc}\,(\Gamma_m) \ll t'_{rad}\,(\Gamma_m) \ll t_{dyn}'$

- the magnetic field may decay on a length scale much shorter than the shocked region scale t'_{dyn} (e.g. Keshet et al. 2009).

Prompt emission models: Pe'er & Zhang 2006; Derishev 2007; Zhao et al. 2014;
Uhm & Zhang 2014; Geng et al. 2018 (much larger scales for B' decay)

Afterglow modelling: Gruzinov 2001; Rossi & Rees 2003; Lemoine 2013

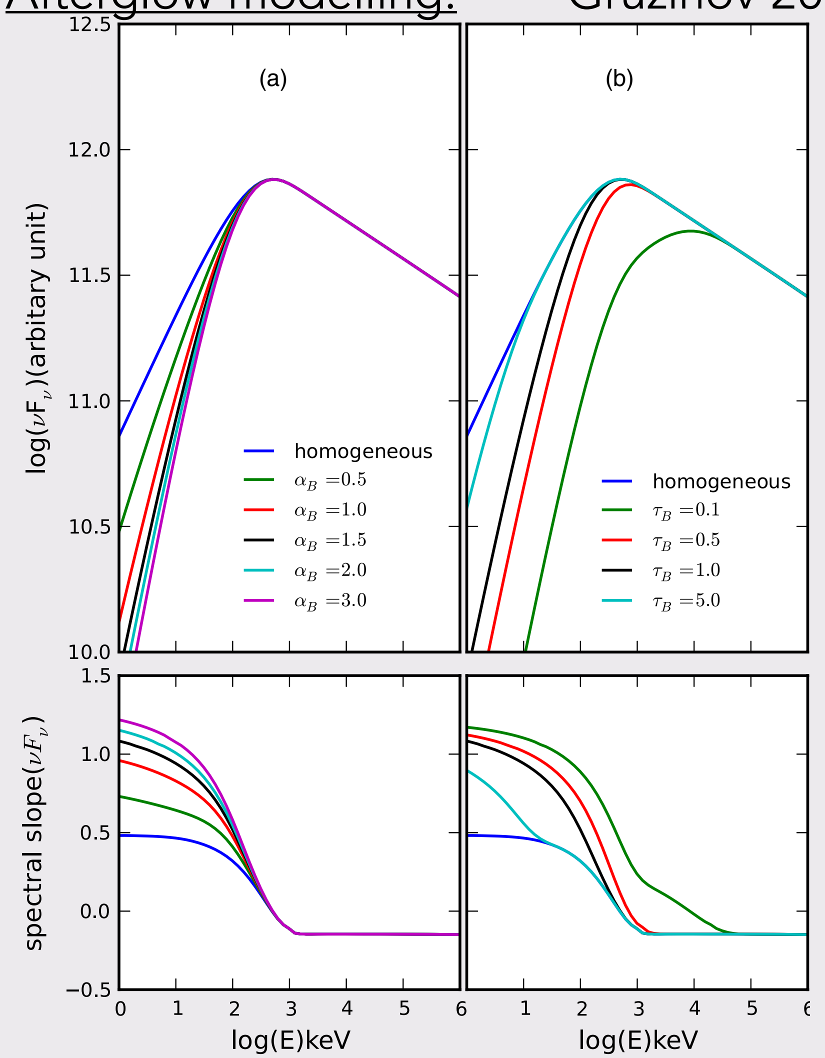

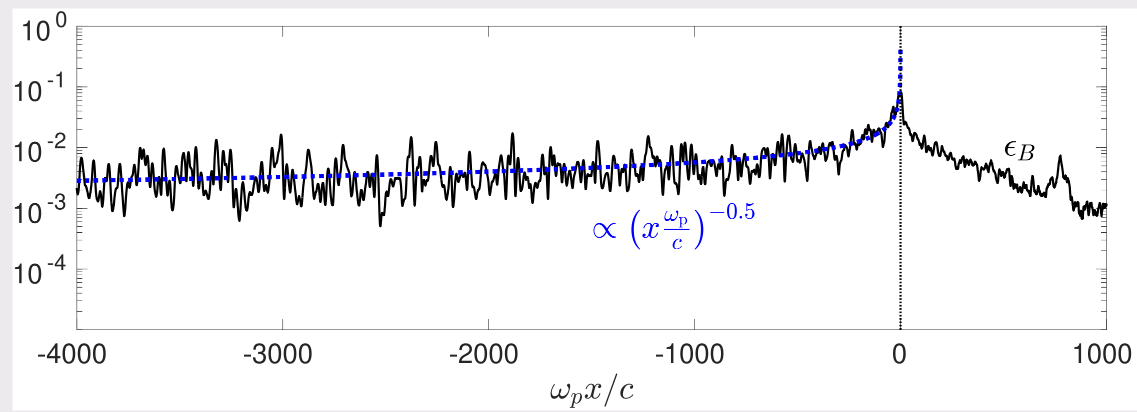

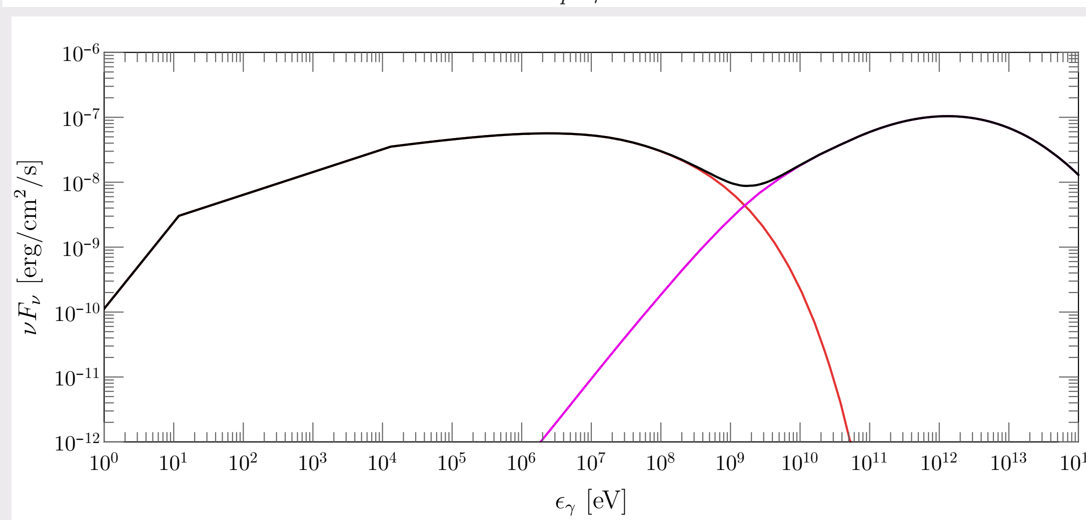

$\epsilon_B = 0.01$
in the shock vicinity
$\epsilon_B \propto (x\ \omega_p / c)^{-0.4}$
$E = 8 \times 10^{53}$ erg
$z = 0.4$
$n = 0.03\ cm^{-3}$
$\epsilon_e = 0.1$
$s = 2.3$
$\gamma_{e,\,max} = 2 \times 10^7$

Vanthieghem et al. 2020:

- decay of the microturbulence in the shocked region
  $\epsilon_B \propto (\,x\ \omega_p/c)^{-0.5}$
- all electrons (but those of the very highest energies) cool in a region in which the turbulence has decayed

Zhao et al. 2014:

PLD & ED models

Klein-Nishina effects neglected

adiabatic cooling not included

Radiative model: exponential decay of the magnetic field

- The magnetic field decay: $B'(t') = B_0' \, e^{-t'/t_B'}$

Electrons radiate efficiently only above an effective Lorentz factor:

$$\Gamma_{c,eff} \simeq \Gamma_{c,0} \, (t'_{dyn} / t'_B)$$

which leads to an increase of the cooling break frequency by a factor $\mathbf{(t_{dyn}'/t_B')^2}$

For an extreme decay, we expect a slow cooling spectrum even for $\Gamma_m > \Gamma_{c,0}$

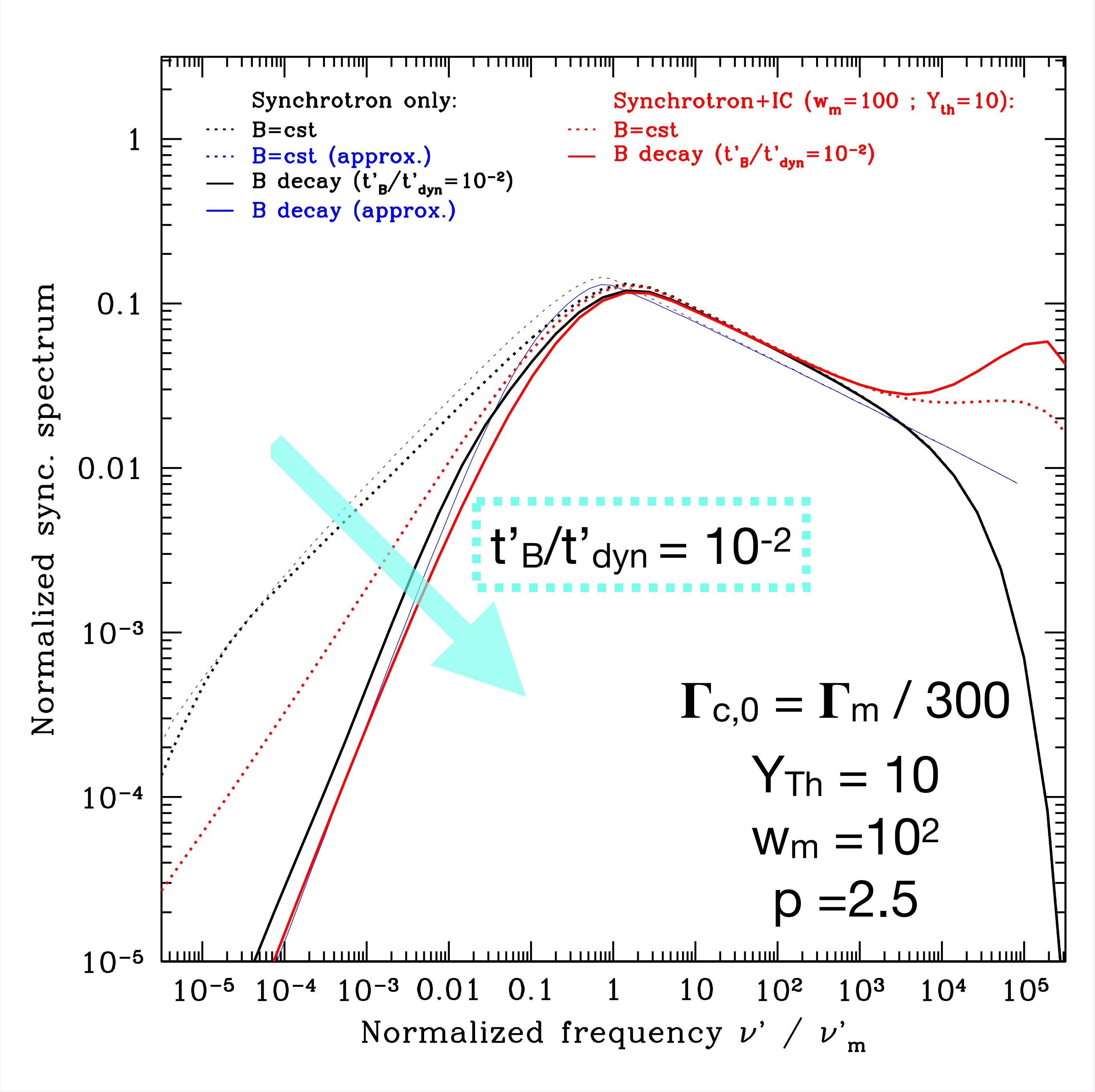

Daigne & Bošnjak 2023, in prep.

Radiative model: exponential decay of the magnetic field

- Evolution of the spectrum as a function of Y_{th} for values of w_m, using a constant magnetic field or a decaying magnetic field on a timescale $t_B'/t_{dyn}' = 0.1$ and 0.01:

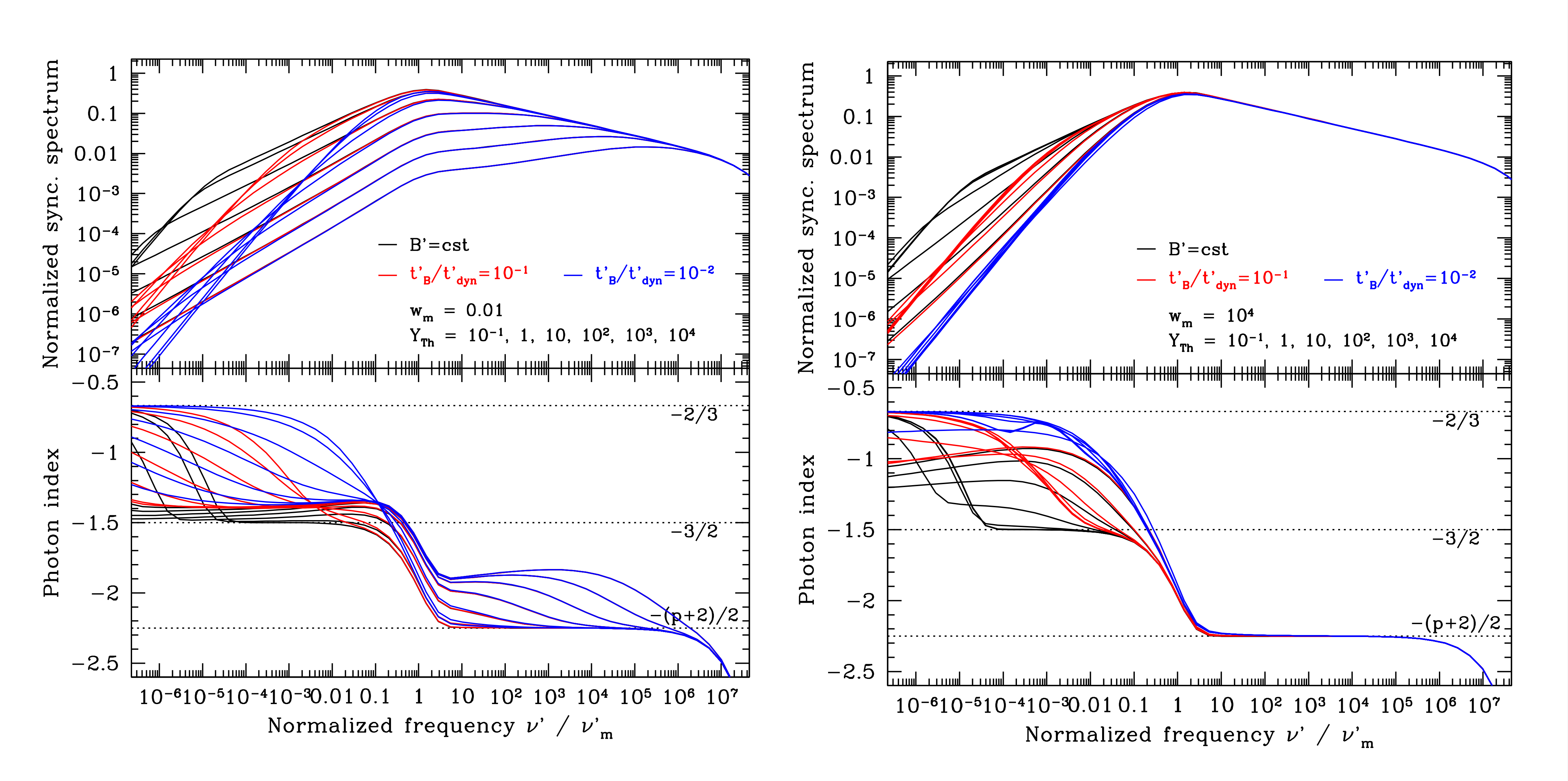

Thomson regime **Klein-Nishina regime**

Daigne & Bošnjak 2023, in prep.

The emitted spectrum in the comoving frame

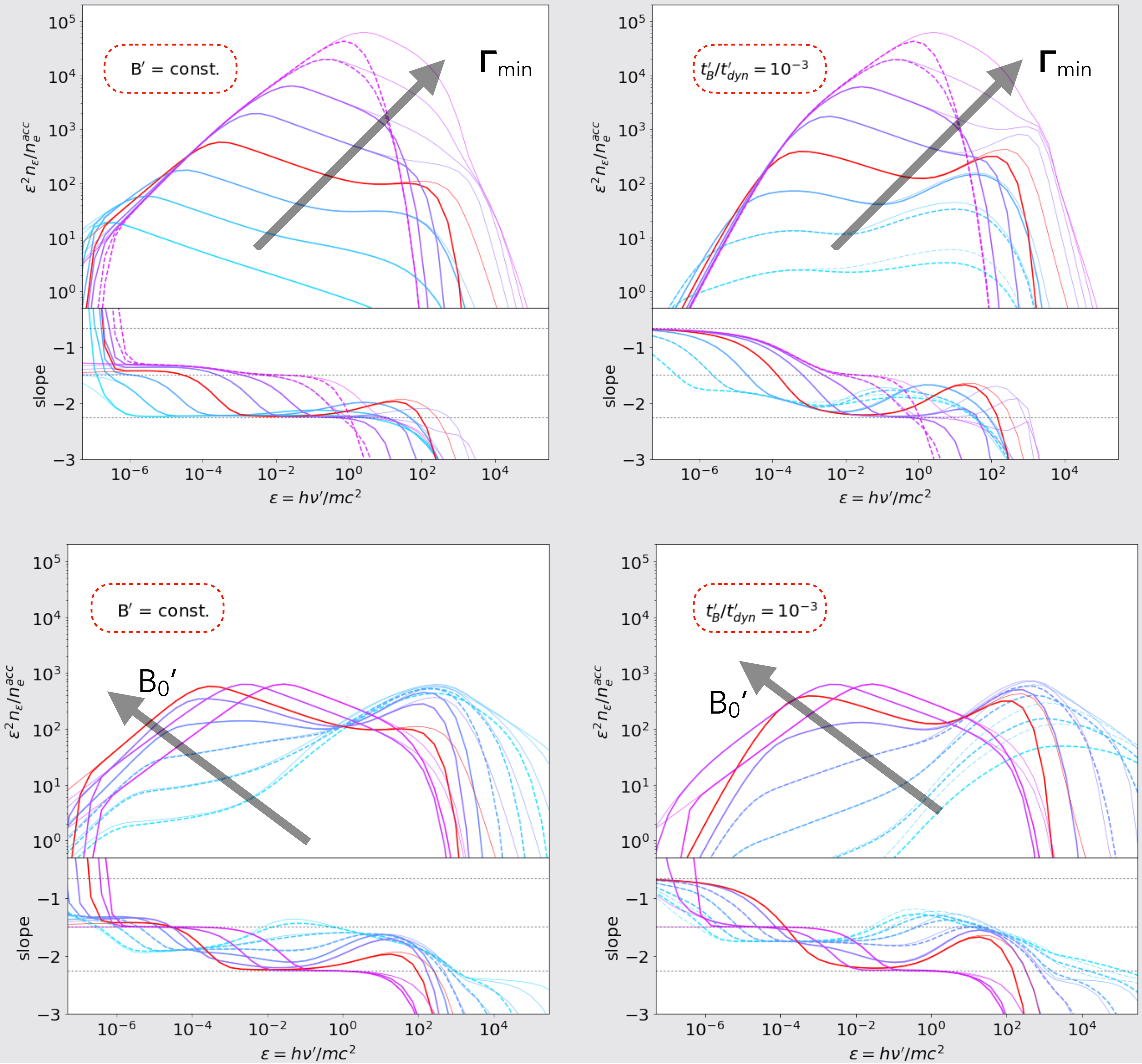

$\tau_{IC} \approx n_e\ (\sigma_T \times \text{KN corr.})\ (c \times t_{rad})$

$Y \approx \tau_{IC} \times (\Gamma_{min}^2 \times \text{KN corr.})$

A strong IC component is obtained when relativistic e- "survive" long enough for scatterings to occur (a low Γ_{min}, a low B′ and a low t_{ex}', i.e. $t_{rad}' \rightarrow t_{ex}'$)

Reference spectrum:

Γ_{min} = 1600

B_0' = 2000 G

$n_e = 4.1 \times 10^7\ cm^{-3}$

t_{dyn} = 80 s

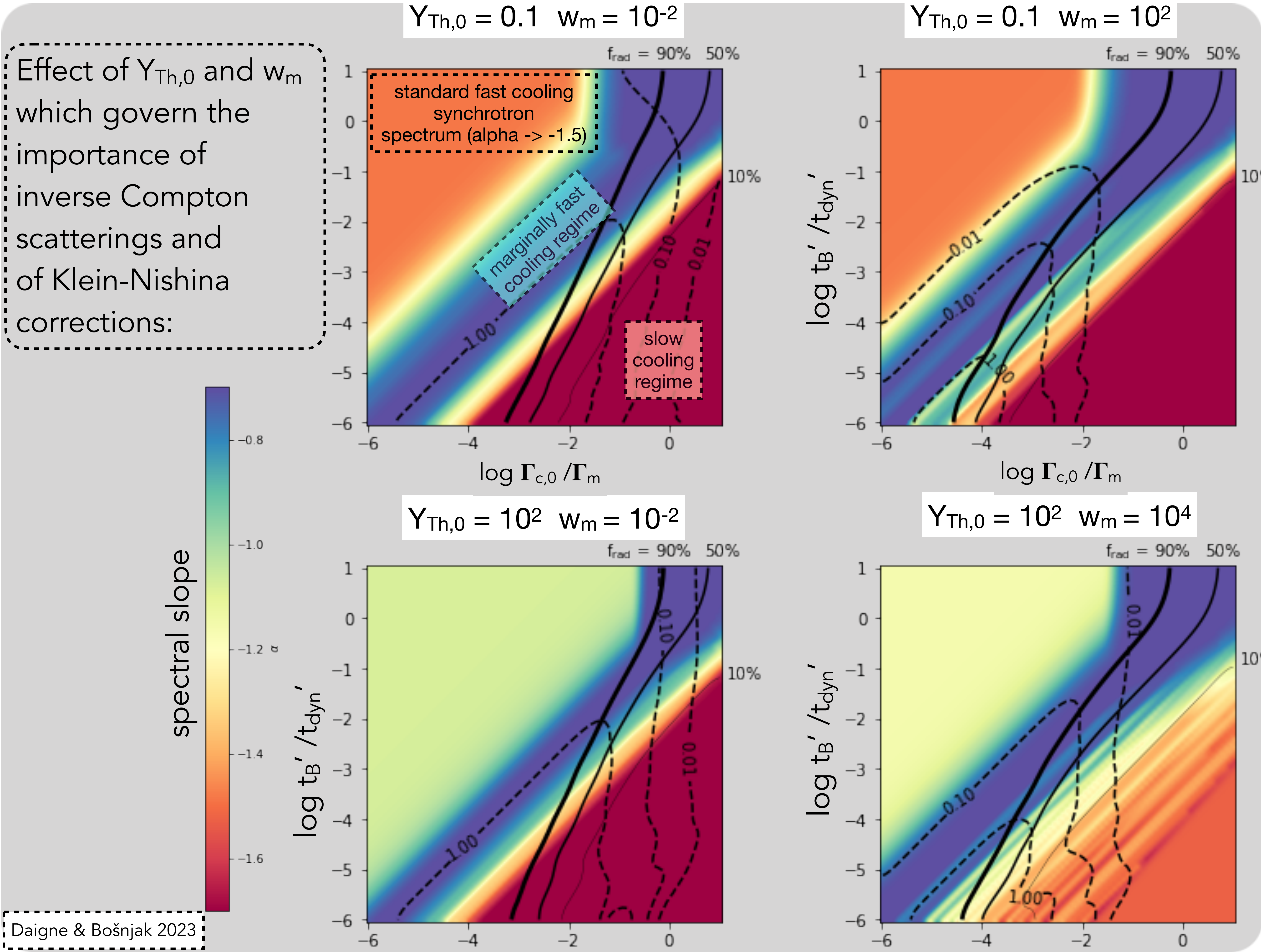

Effect of $Y_{Th,0}$ and w_m which govern the importance of inverse Compton scatterings and of Klein-Nishina corrections:
$Y_{Th,0} = 0.1 \quad w_m = 10^{-2}$
$Y_{Th,0} = 0.1 \quad w_m = 10^{2}$
$Y_{Th,0} = 10^{2} \quad w_m = 10^{-2}$
$Y_{Th,0} = 10^{2} \quad w_m = 10^{4}$
f_{rad} = 90% 50%
10%
standard fast cooling synchrotron spectrum (alpha -> -1.5)
marginally fast cooling regime
slow cooling regime
1.00
0.10
0.01
$\log \Gamma_{c,0} / \Gamma_m$
$\log t_B' / t_{dyn}'$
spectral slope
α
Daigne & Bošnjak 2023

Internal shock model

The jet is assumed to be weakly magnetized at large distance and the prompt emission is emitted above the photosphere by shock accelerated electrons.

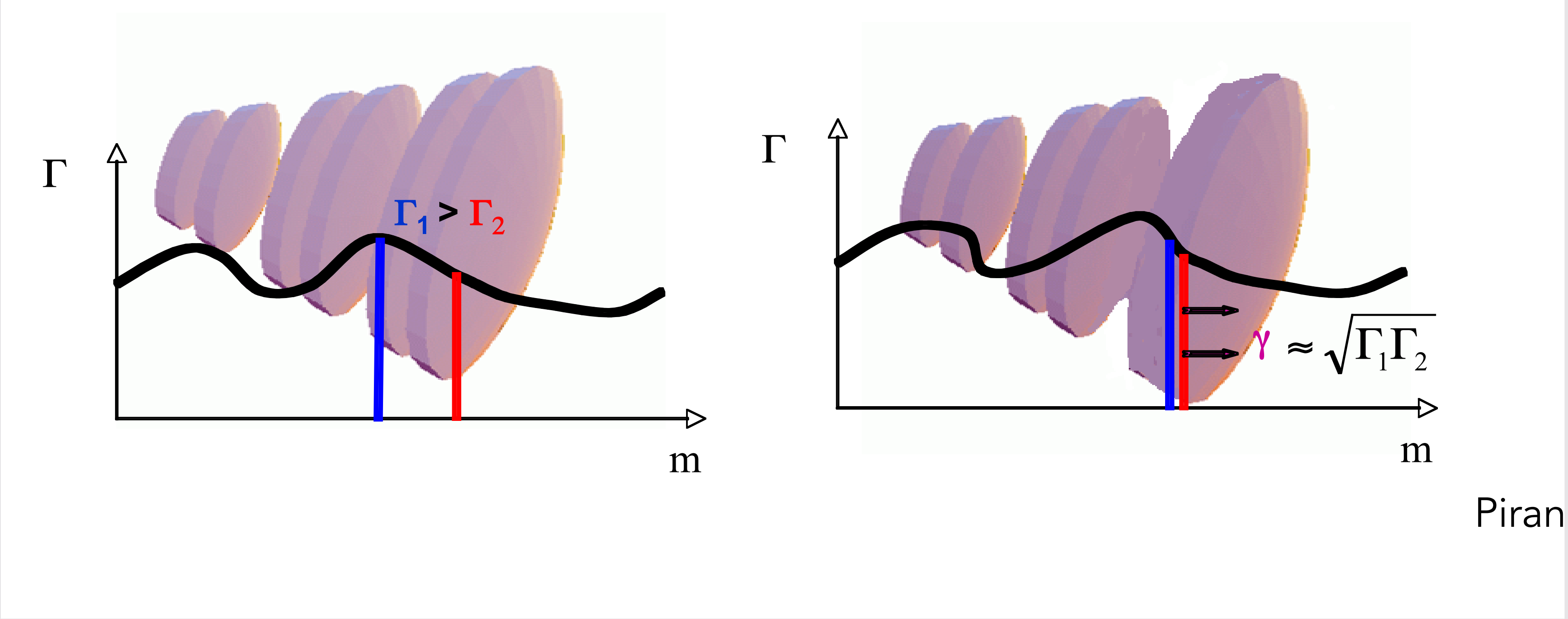

Piran 1999

Modeling:

1. dynamics of internal shocks

2. radiative processes in the shocked medium

3. observed spectra and time profiles

Bosnjak, Daigne & Dubus 2009
Daigne, Bosnjak & Dubus 2011
Bosnjak & Daigne 2014

Internal shock model

Physical conditions in the shocked medium: Lorentz factor $\mathbf{\Gamma^*}$, comoving density ρ^*, comoving specific energy density ε^*

Relativistic electron density:

$$n'(\Gamma_e, t'=0) \propto \Gamma_e^{-p} \qquad \Gamma_e \geq \Gamma_m$$

$\zeta < 1$ of all electrons is accelerated

Bykov & Meszaros 1996
Spitkovsky 2008

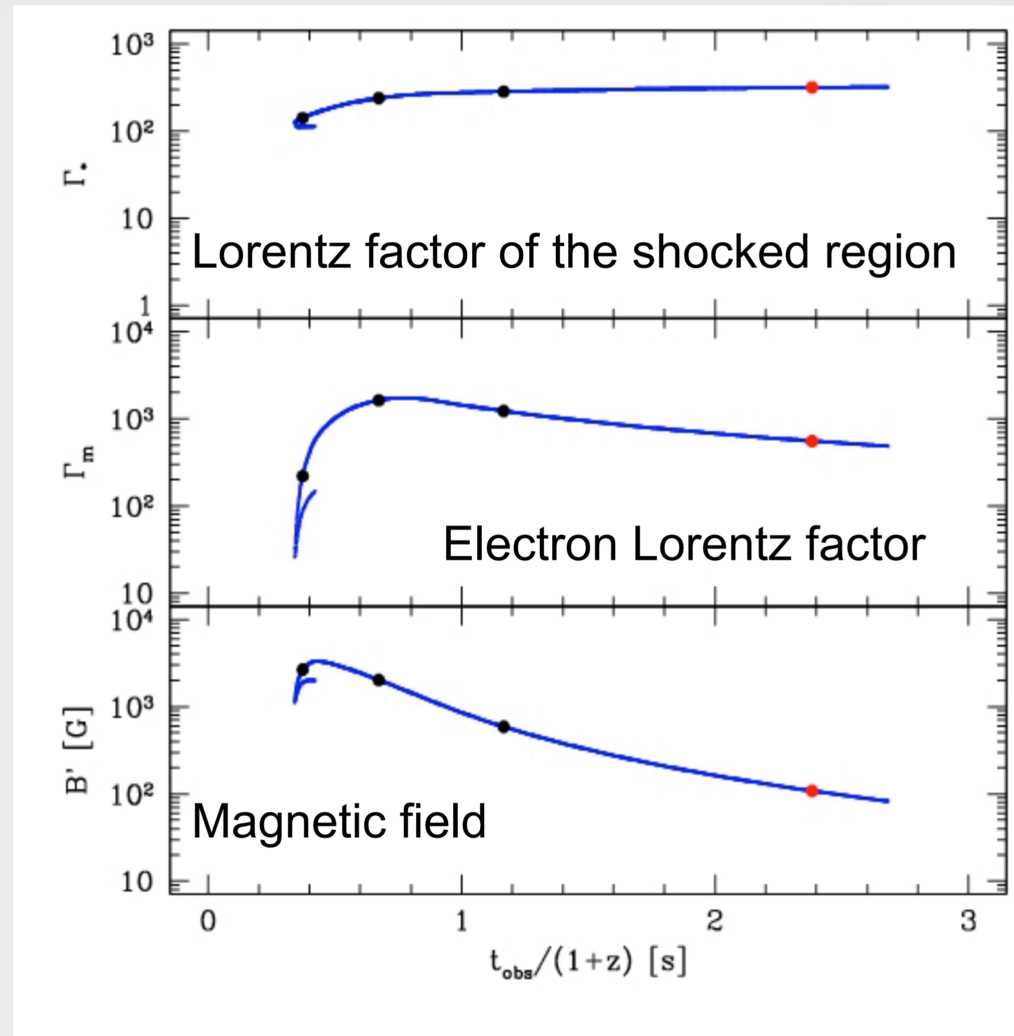

Dissipated energy is distributed between protons, electrons (fraction ε_e) and magnetic field (fraction ε_B)

Spectral evolution in the internal shock model: steep low energy slopes

Case A: a single pulse burst with a high magnetic field. The main spectral peak is due to synchrotron emission (Bošnjak, Daigne & Dubus 2009)

$\epsilon_B = 1/3$, $\epsilon_e = 1/3$, $\xi = 3 \times 10^{-3}$, $p = 2.5$, $dE/dt = 5 \times 10^{53}$ erg/s

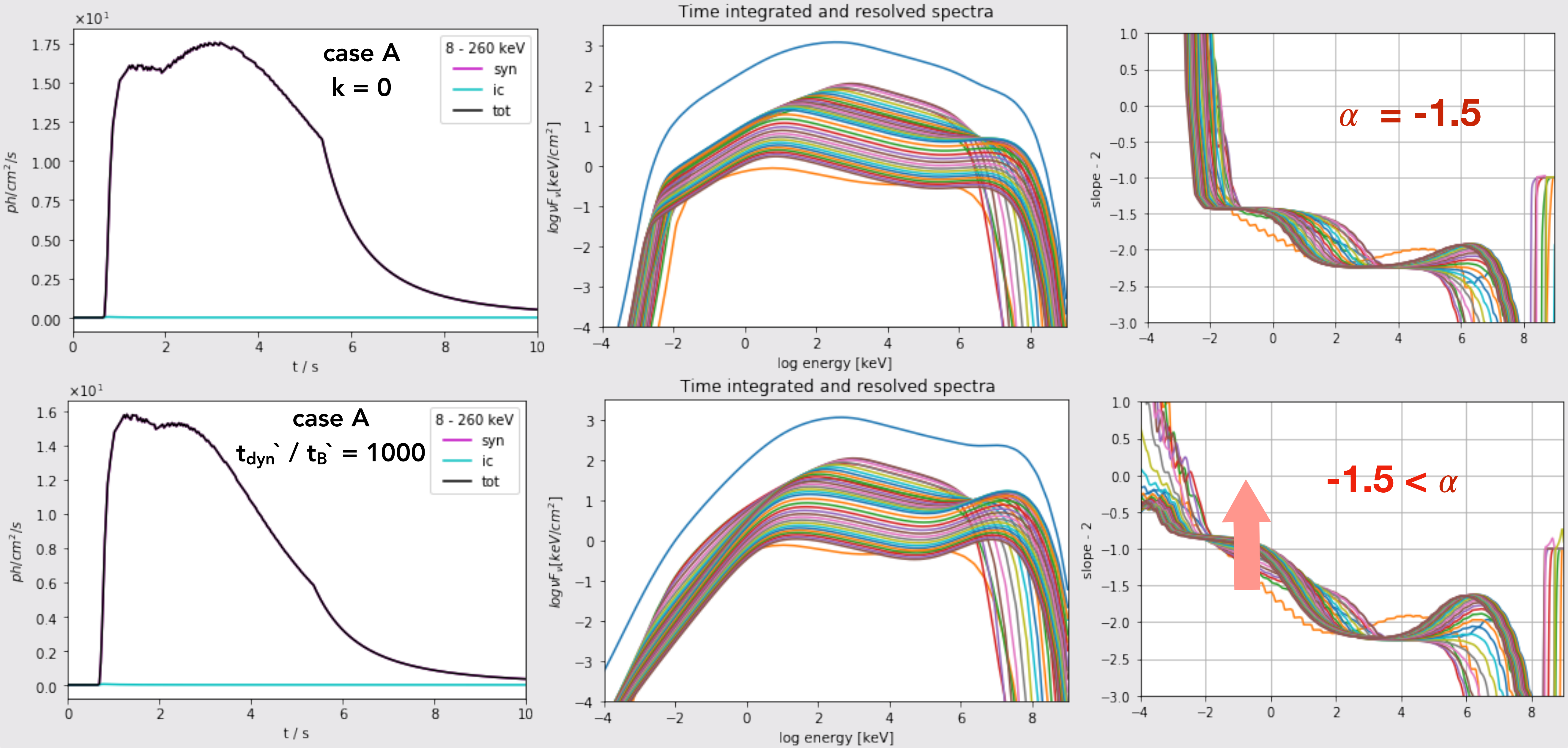

Spectral evolution in the internal shock model: steep low energy slopes

Case B: a single pulse burst with a low magnetic field. The main spectral peak is due to synchrotron emission (Bošnjak, Daigne & Dubus 2009)

$\epsilon_B = 5 \times 10^{-3}$, $\epsilon_e = 1/3$, $\xi = 2 \times 10^{-3}$, $p = 2.5$, $dE/dt = 5 \times 10^{53}$ erg/s

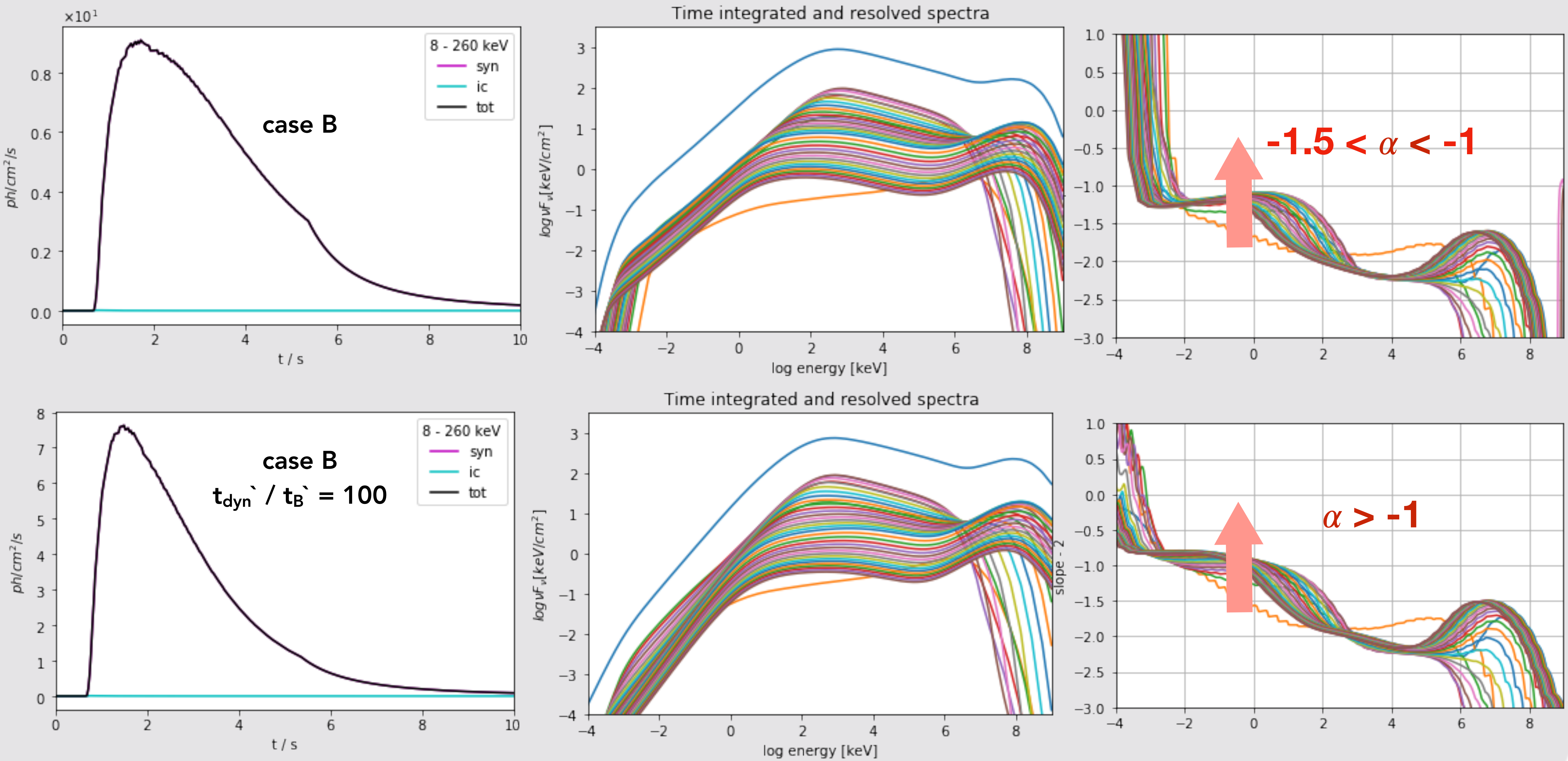

Effect of a decaying magnetic field in the internal shock model: reference case B with $t_B/t_{dyn} = 10^{-3}$:

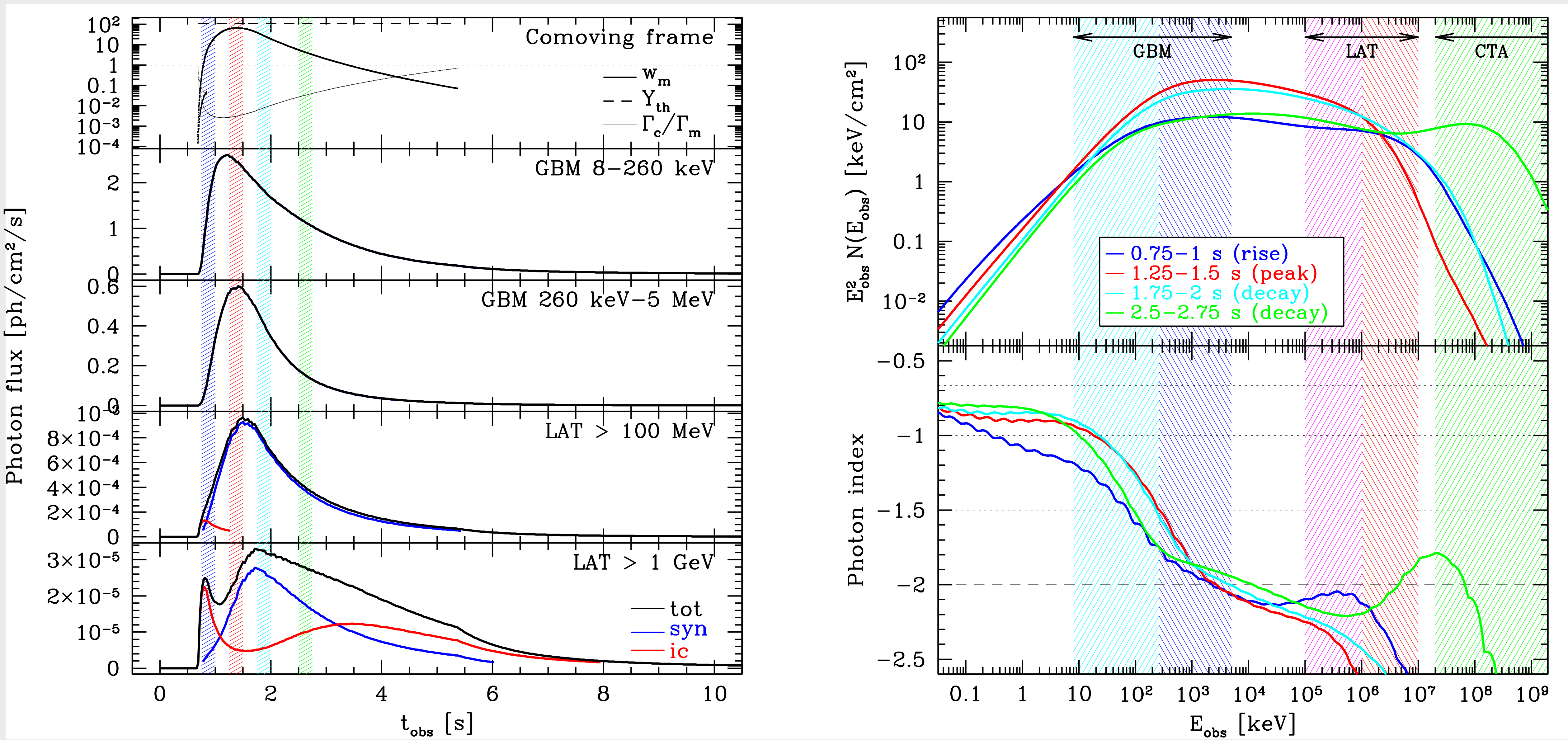

Daigne & Bošnjak 2023

Lepto-hadronic model

Rudolph, Petropoulou, ŽB, Winter 2023
Rudolph, Petropoulou, Winter, ŽB 2023

AM³ time-rependent code (Gao et al. 2017) following the coupled evolution of photons, electrons, positrons, muons, pions, p, n, and ν
All relevant nonthermal processes included: synchrotron emission, SSA, IC scatterings, photopair and photopion production, $\gamma\gamma$-annihilation, adiabatic cooling & escape

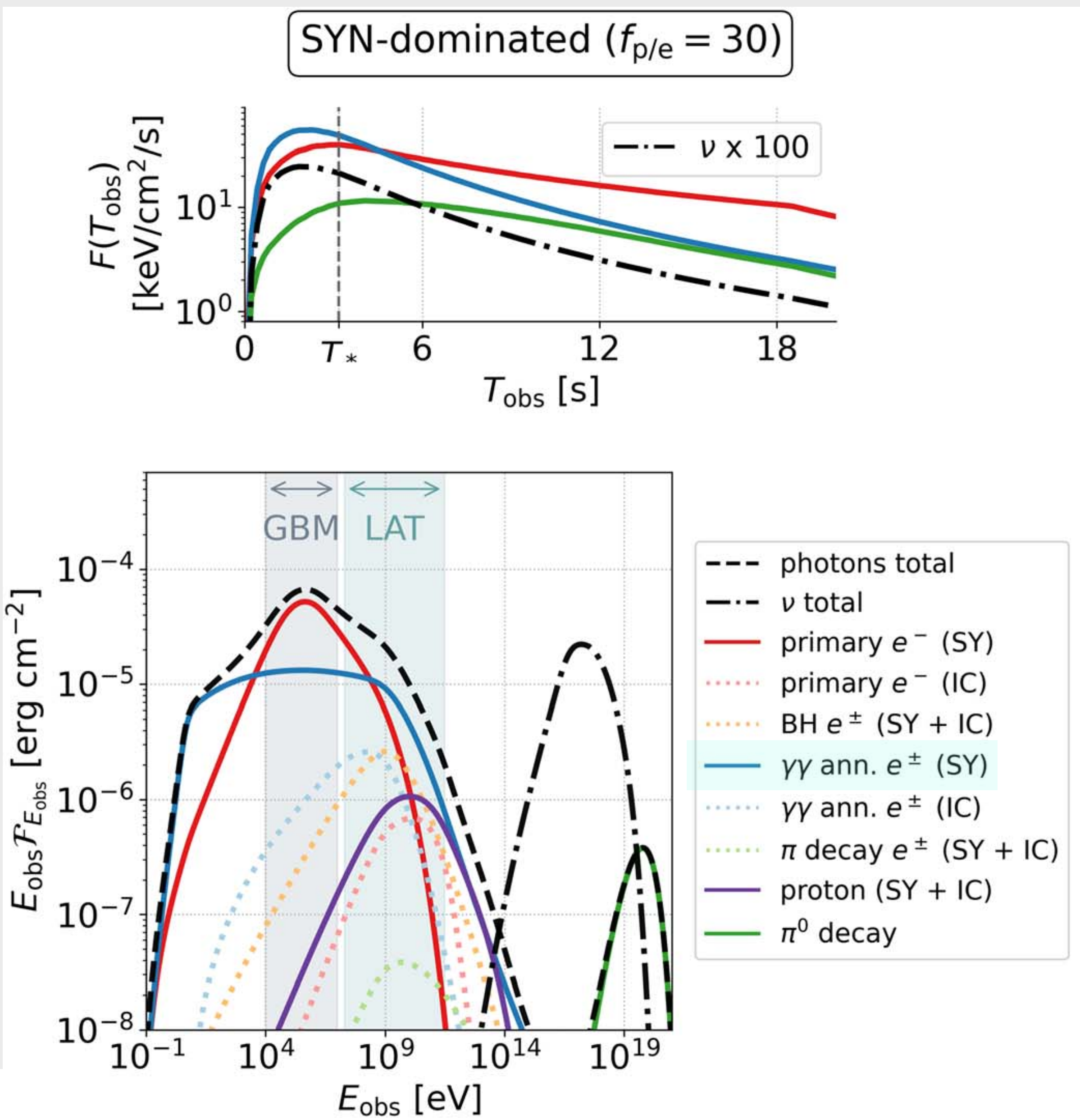

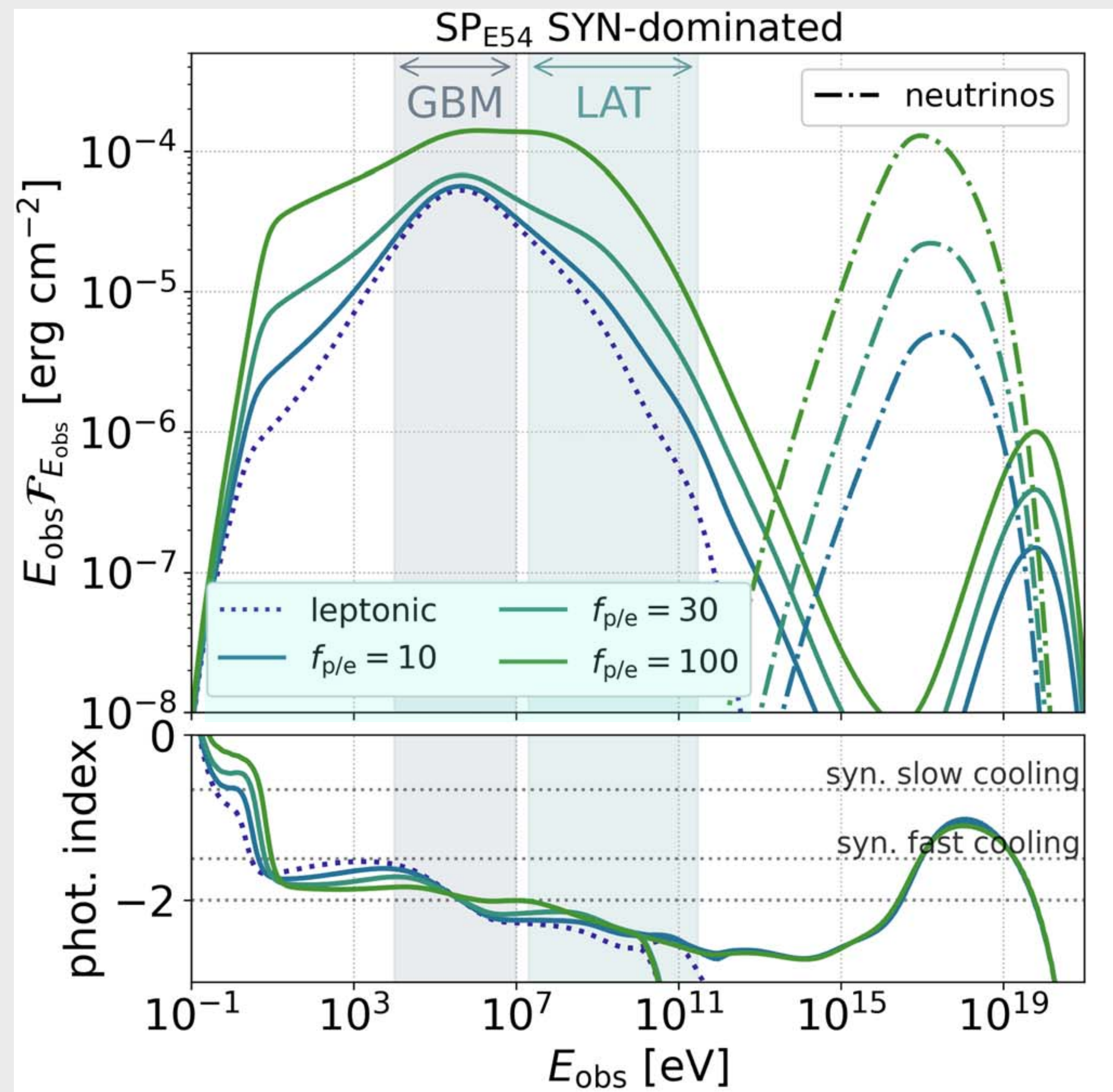

GRB 221009A

Locations of the dust layers associated with the five smallest X-ray rings from the GRB 221009A:

- GRB occurred at low Galactic latitude

The direction to the burst; dark patches represent the dust layers responsible for producing the X-ray rings

- the smallest ring corresponds to the most distant dust

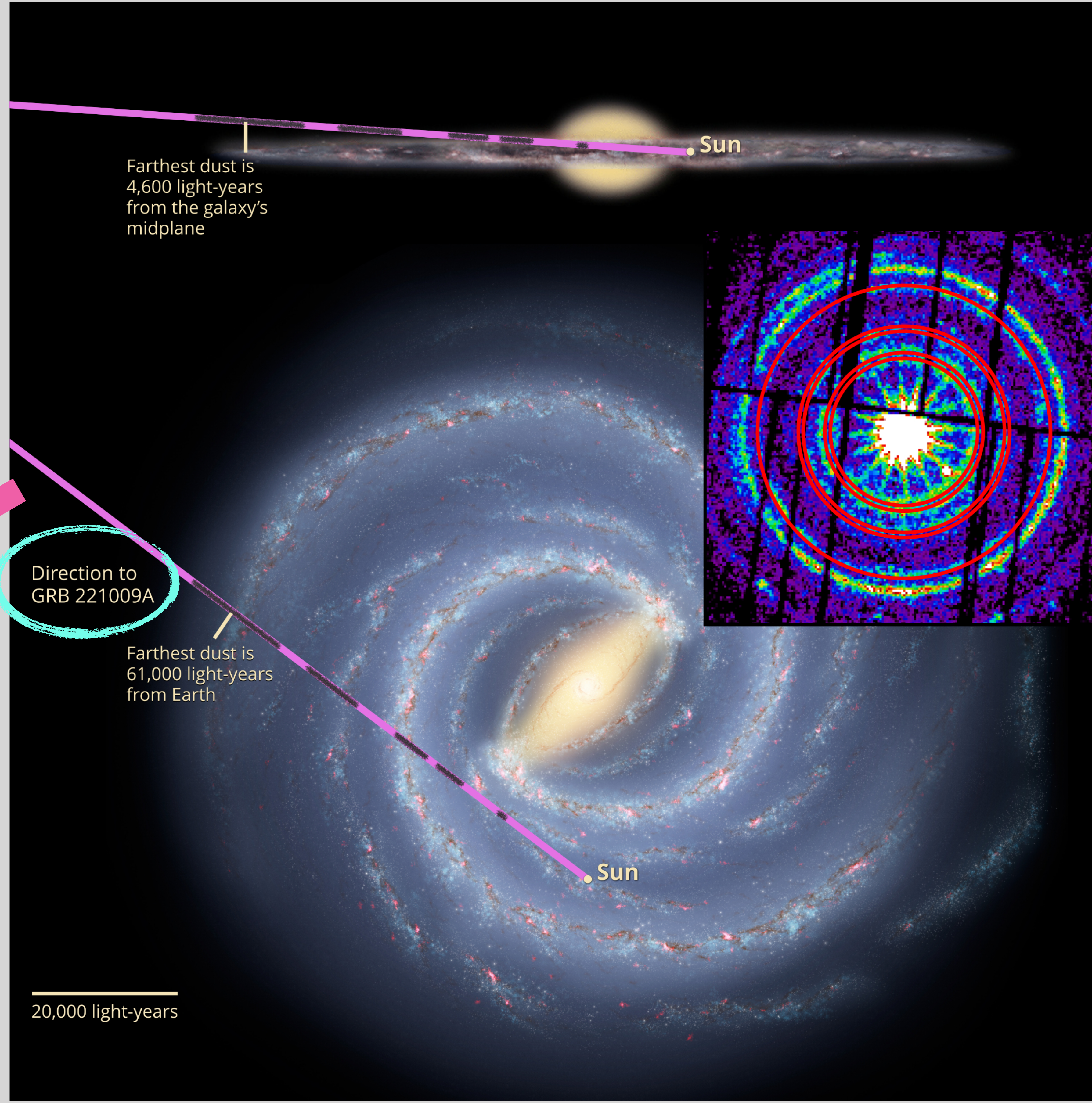

Credit: NASA's Goddard Space Flight Center

GRB 221009A

GRB 221009A: EPIC 0.7-4 keV images [counts/s/arcmin^2] of the expanding rings

The two red circles of radii 8′ and 11′ : a reference for ring expansion.

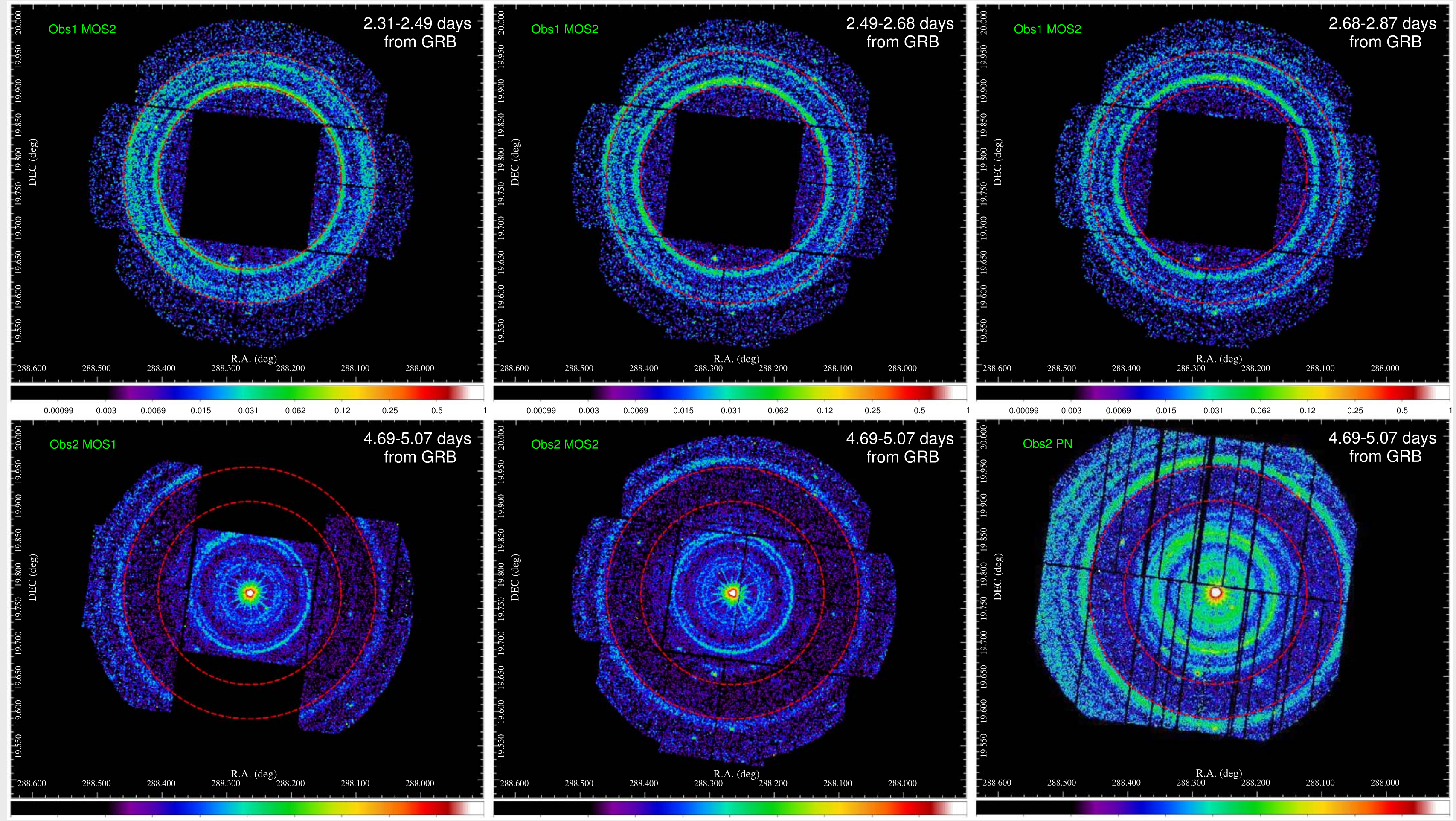

Tiengo, Pintore, ..ŽB, Jelić, Campana 2023
Šiljeg, ŽB, Jelić, Tiengo et al. 2023

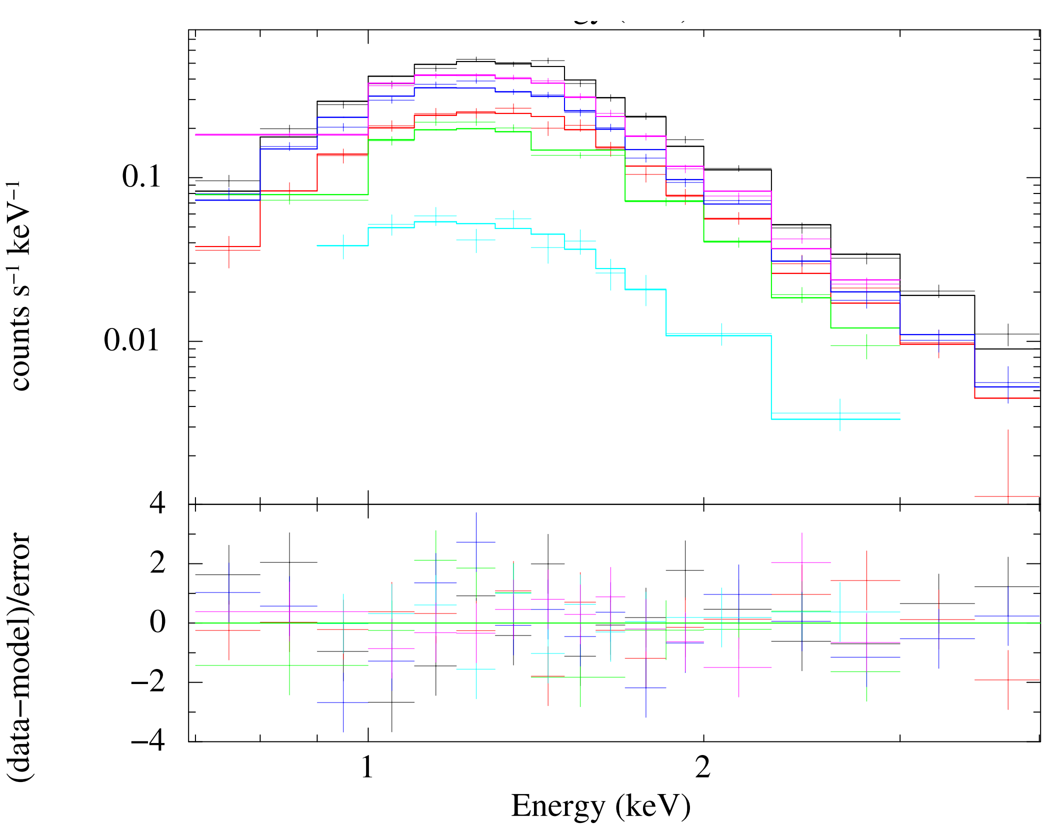

MOS2 spectra of rings 1-6 (Tiengo et al. 2023)

By fitting the spectra of the rings with different models for the dust composition and grain size distribution —> the spectrum of the GRB prompt emission in the 0.7 - 4 keV as an absoprbed power law with photon index **Γ** =1 -1.4

The photon index and the fluence indicate the presence of a possible soft excess with respect to the extrapolation of the main GRB peak!

Summary - I

When the characteristic decay length of the magnetic field ($B \propto e^{-t'/t_B'}$) is significantly shorter than the dynamical scale ($t_B'/t_{dyn}' \sim 0.01, 0.001$) , the low energy prompt GRB synchrotron spectrum becomes significantly harder. The regime of marginally fast cooling is naturally achieved

If the magnetic field decays extremely fast ($t_B'/t_{dyn}' \ll \Gamma_{c,0} / \Gamma_m$), the low energy photon index -2/3 is still recovered, but all electrons may be slow cooling leading to a lower radiative efficiency

A future work will investigate how t_B' should evolve with physical conditions in the shocked medium and what are the consequences for the spectral evolution

If the low energy emission spectrum can be reconstructed as e.g. from X-ray halo observations, potentially the hadronic-related contribution could be constrained

II. Off-axis MeV and very-high energy gamma-ray emissions from structured gamma-ray burst jets

- **Motivation**

  Ioka & Nakamura (2018) : the short GRB 170817A (detected ~ 1.7 s after the gravitational wave event GW 170817) is faint because the jet is off-axis to our line of sight

Off-axis observer receives photons emitted outside the beaming cone. Consequently, the apparent energy of the off-axis jet becomes faint.

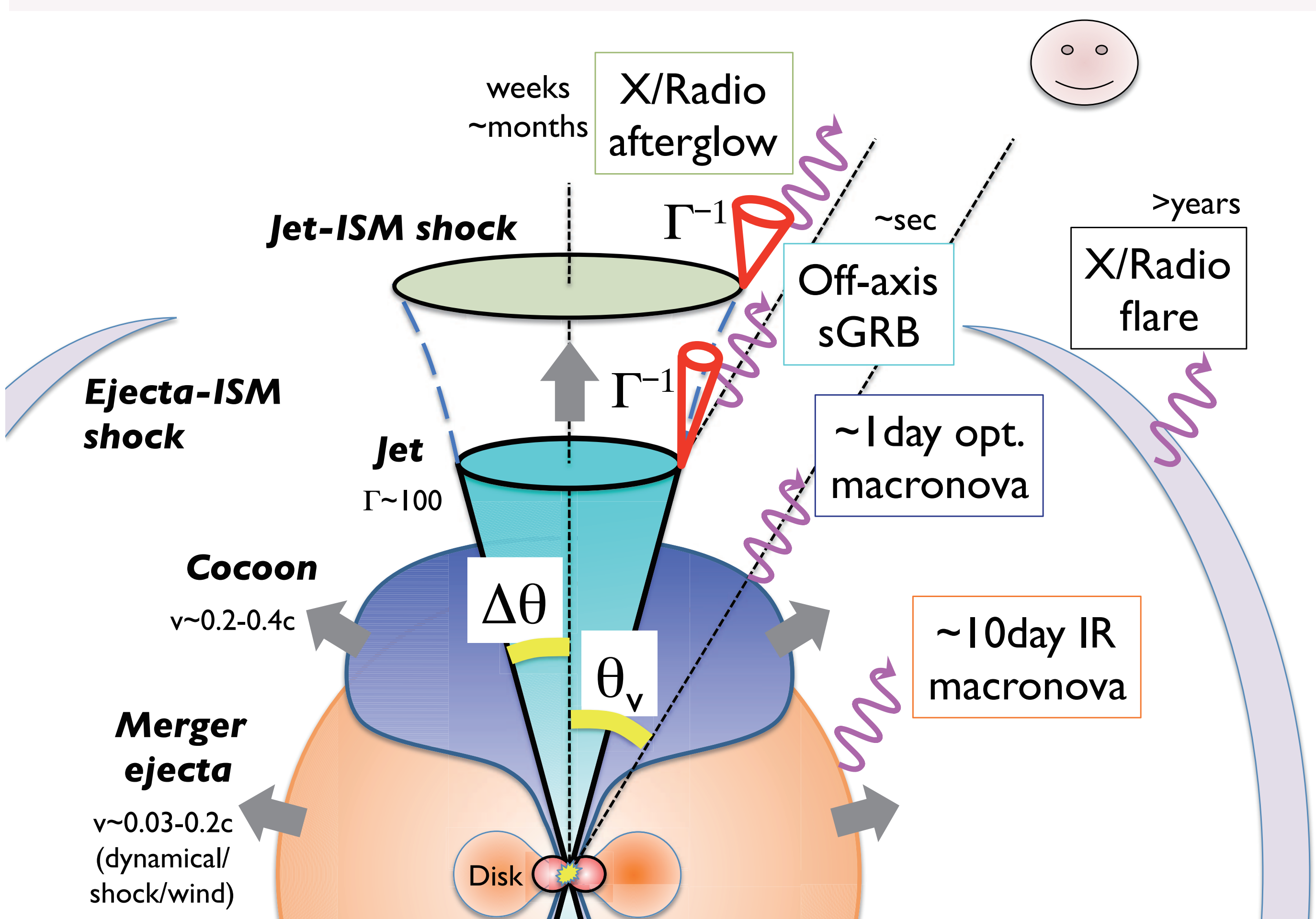

Ioka & Nakamura 2018

1. a binary NS merger is at the origin of sGRB E_{iso} = 5.35 x 10^{46} erg

2. sGRB produces an afterglow via interaction with the interstellar medium. For off-axis observers, the early afterglow looks faint

3. a small amount of NS material ejected from the NS merger is expected to emit optical-IR signal ('kilonova')

4. a radio flare and the associated X-ray remantns occur through the interaction between the merger ejecta and the ISM

- **Motivation**

The off-axis model was initially studied by using a top-hat jet with uniform brightness and a sharp edge. However, it is difficult to explain ν_{peak} = 185 ± 62 keV + the slowly rising afterglow light curve is not consistent with a top-hat jet (Moolet et al. 2018), but strongly suggests a structured jet

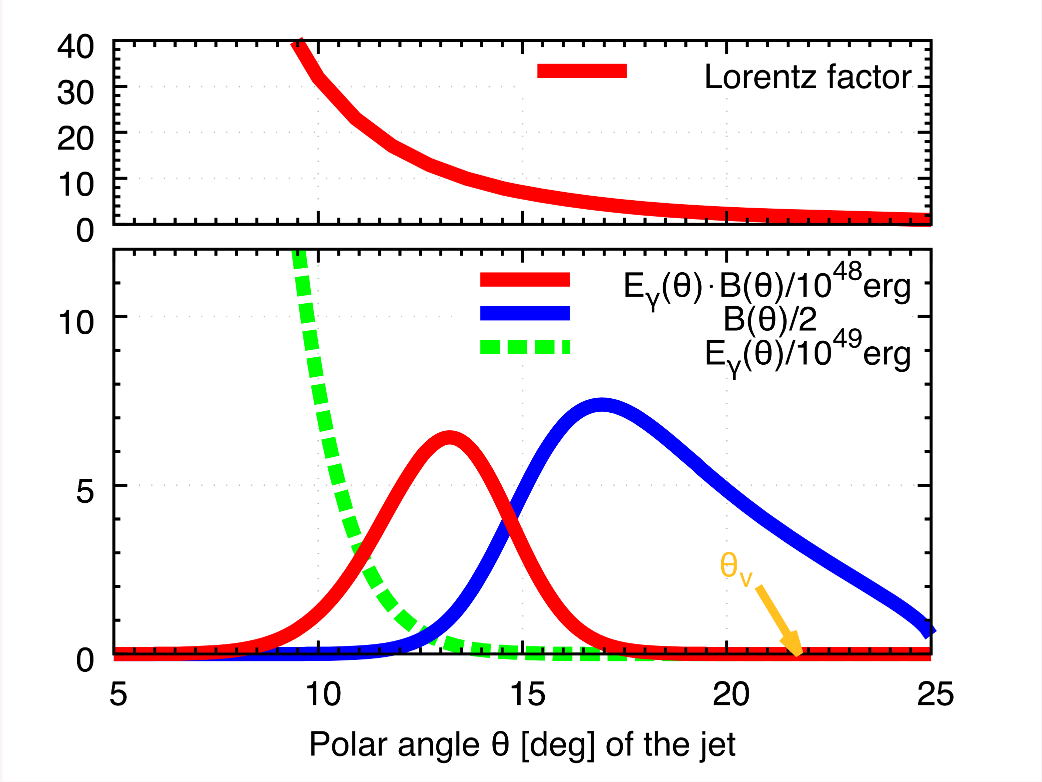

$$\Gamma = \frac{\Gamma_{\rm max}}{1+(\theta/\theta_{\rm c})^{\lambda}}$$

Ioka & Nakamura 2019

Isotropic gamma-ray energy of the jet decreases exponentially outward:

$$E_\gamma(\theta) = \epsilon_\gamma E_0 \exp(-\theta^2/2\theta_{\rm c}^2)$$

$E_o = 10^{52.8}$ erg $\theta_c = 0.059$ n = $10^{-2.51}$ cm^{-3} $\theta_v = 0.38 \approx 22^{\circ}$ (Troja et al. 2018)

- **Off-axis emission from a structured jet**

The surface brightness
(the isotropic energy per solid angle):

$$\frac{dE_{\gamma,\mathrm{iso}}}{d\Omega} = \frac{1}{4\pi}\frac{E_\gamma(\theta)}{\Gamma^4(1-\beta\cos\theta_\Delta)^3}$$

$$\cos\theta_\Delta = \sin\theta\cos\phi\sin\theta_v + \cos\theta\cos\theta_v$$

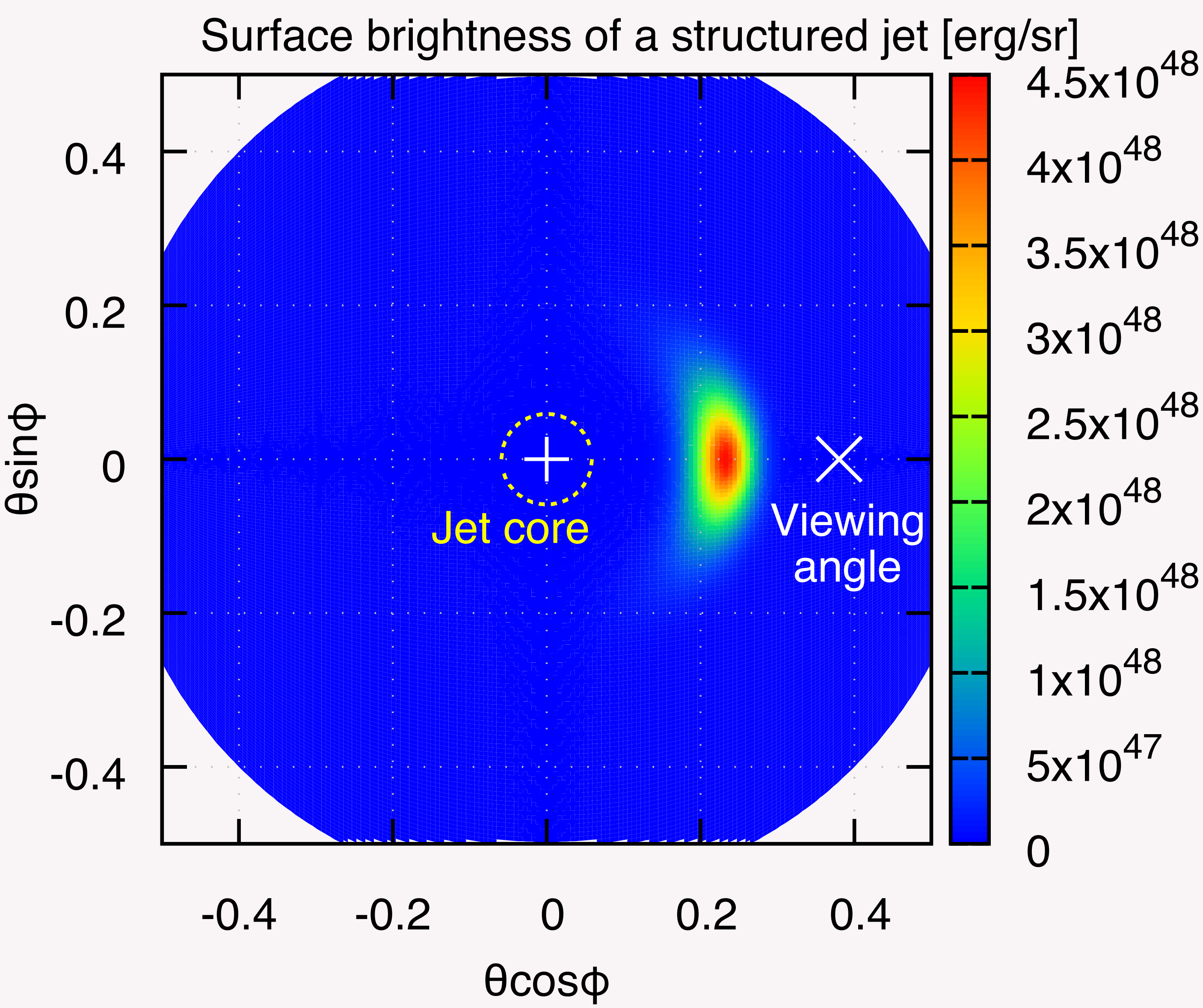

The off-axis model for GRB 170817A predicted that the most luminous region arises neither from the jet core, nor at the line of sight at the viewing angle, but from the off-centre jet.

Ioka & Nakamura 2019

II. Off-axis MeV and very-high energy gamma-ray emissions from structured gamma-ray burst jets

- **TeV photons**

The different energy photons (MeV, TeV) arrive to the observer from different emission zones for off-axis structured jets, mainly due to the effect of the two-photon pair annihilation process

The optical depth for VHE photons is much higher in the core region near the jet surface, which gradually decreases outwards allowing VHE photons to escape.

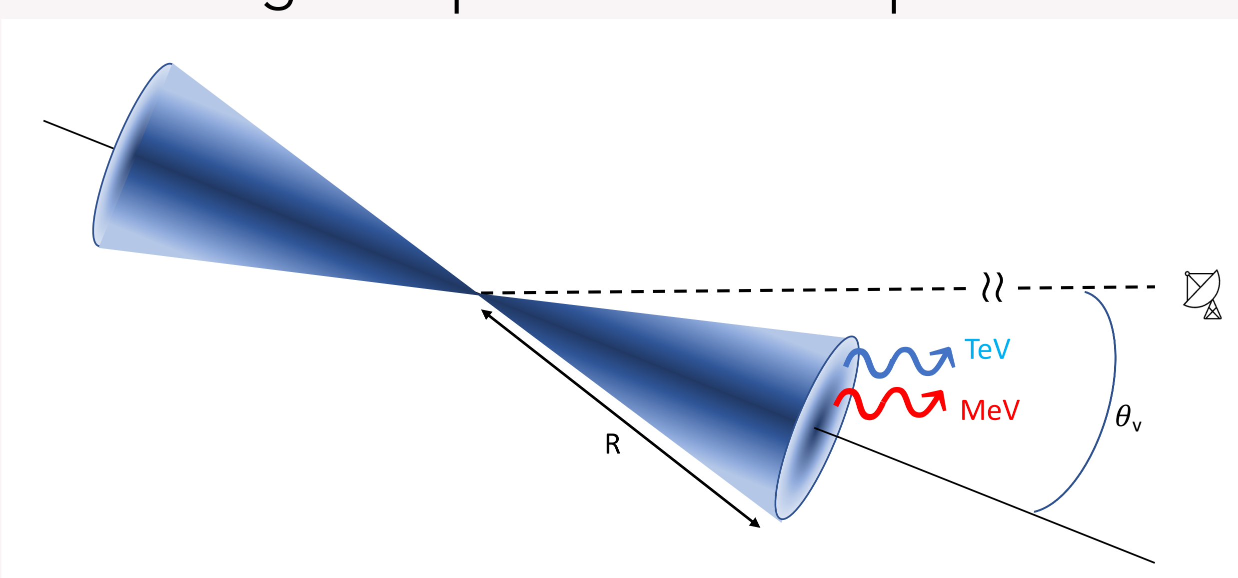

ŽB, Zhang, Murase, Ioka 2023

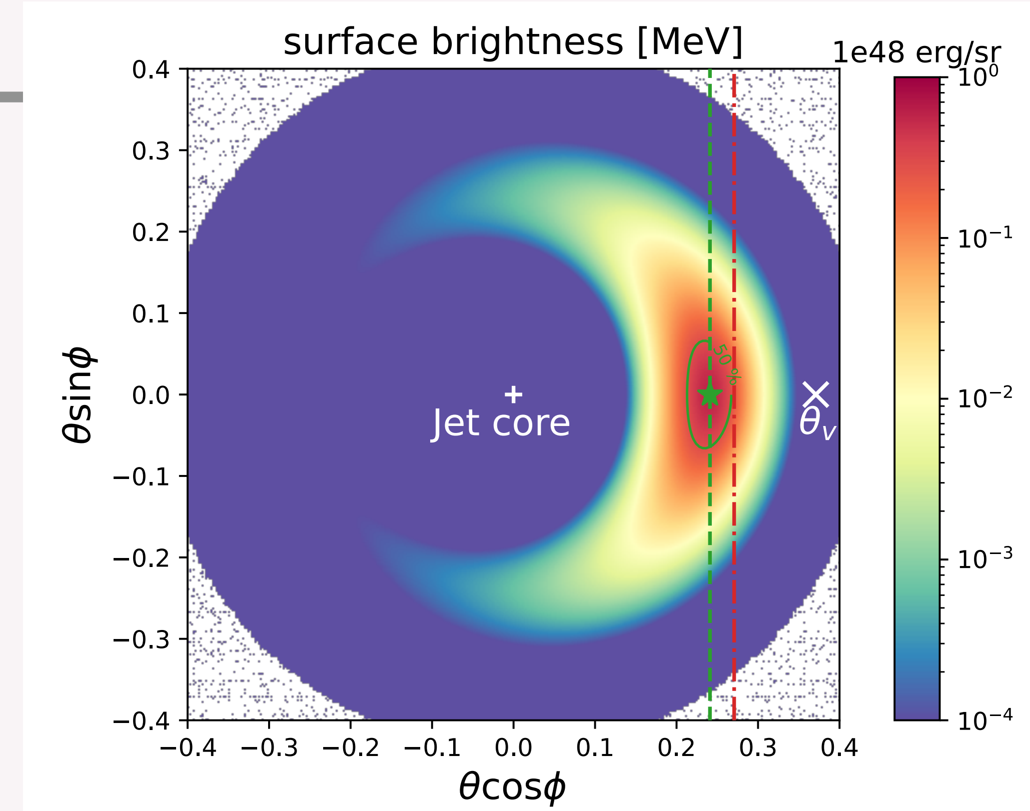

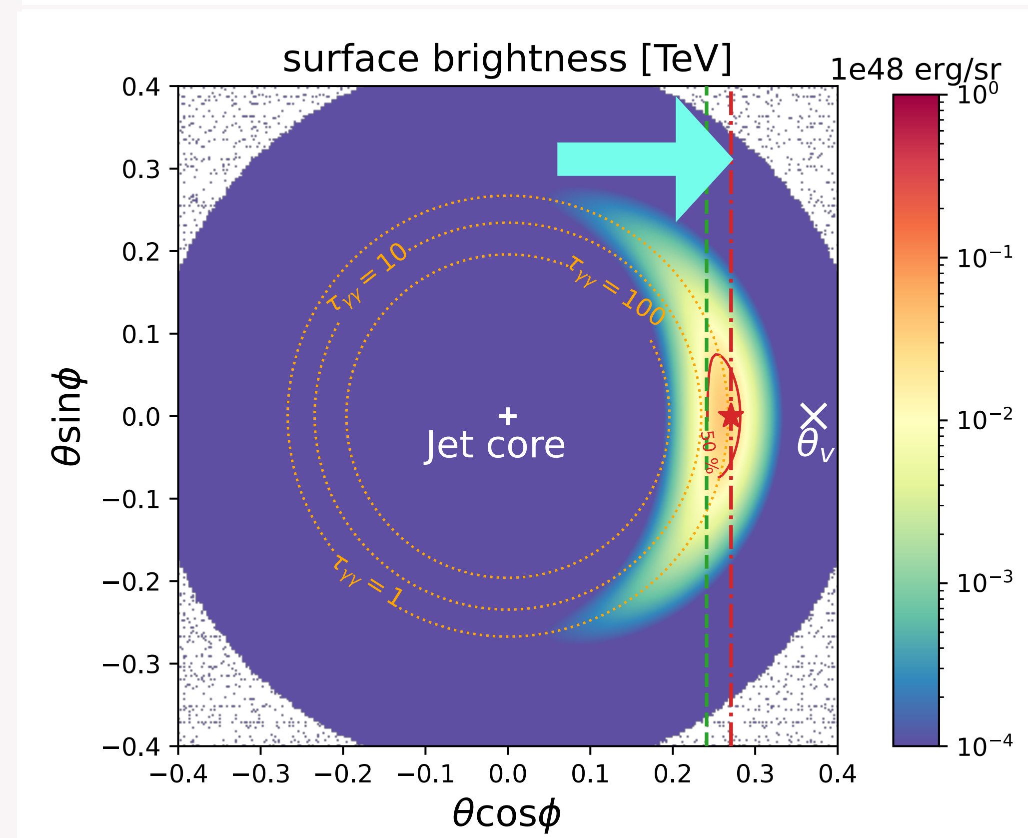

Emission regions with 50% surface brightness are shifted between the MeV and TeV bands!

- **TeV photons**

The optical depth is sensitive to the emission radius: the corresponding time delay between the typical arrival time of the TeV and MeV emission decreases with the increase of the emission radius.

ŽB, Zhang, Murase, Ioka 2023

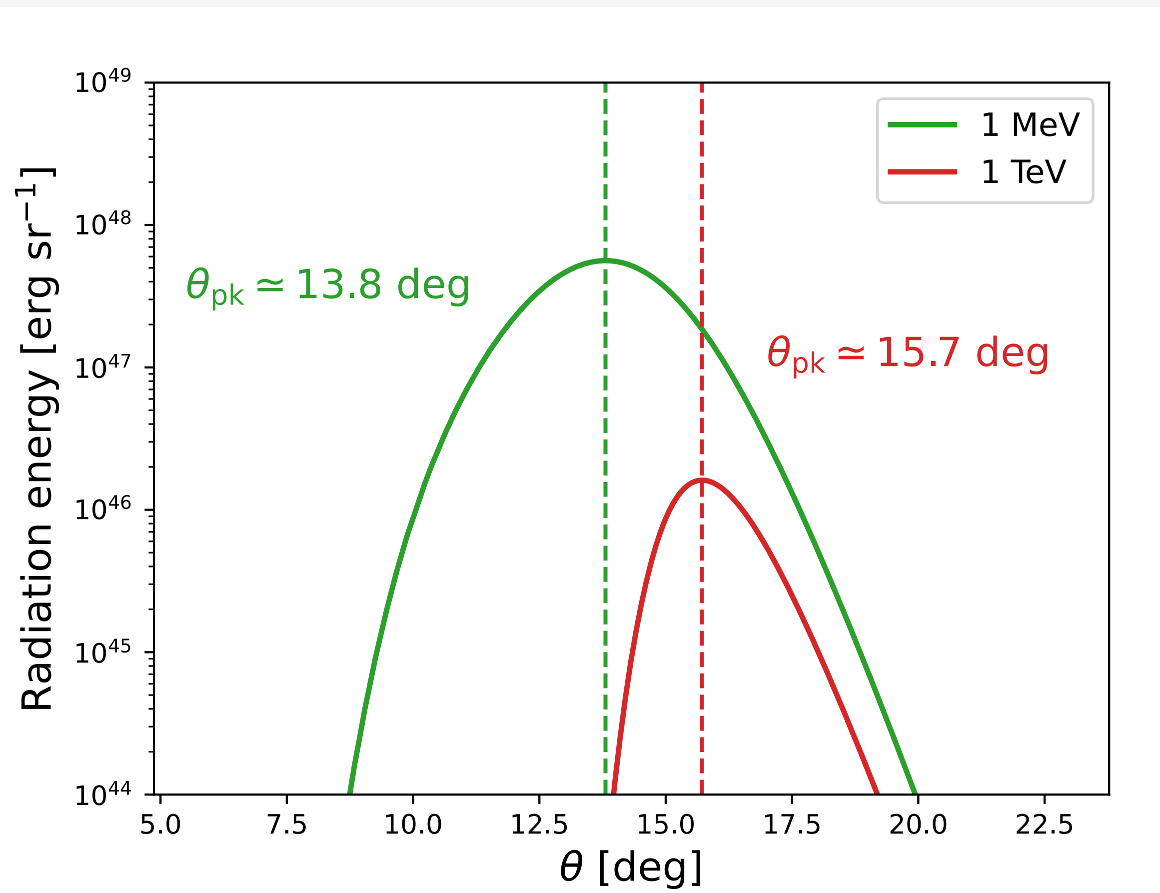

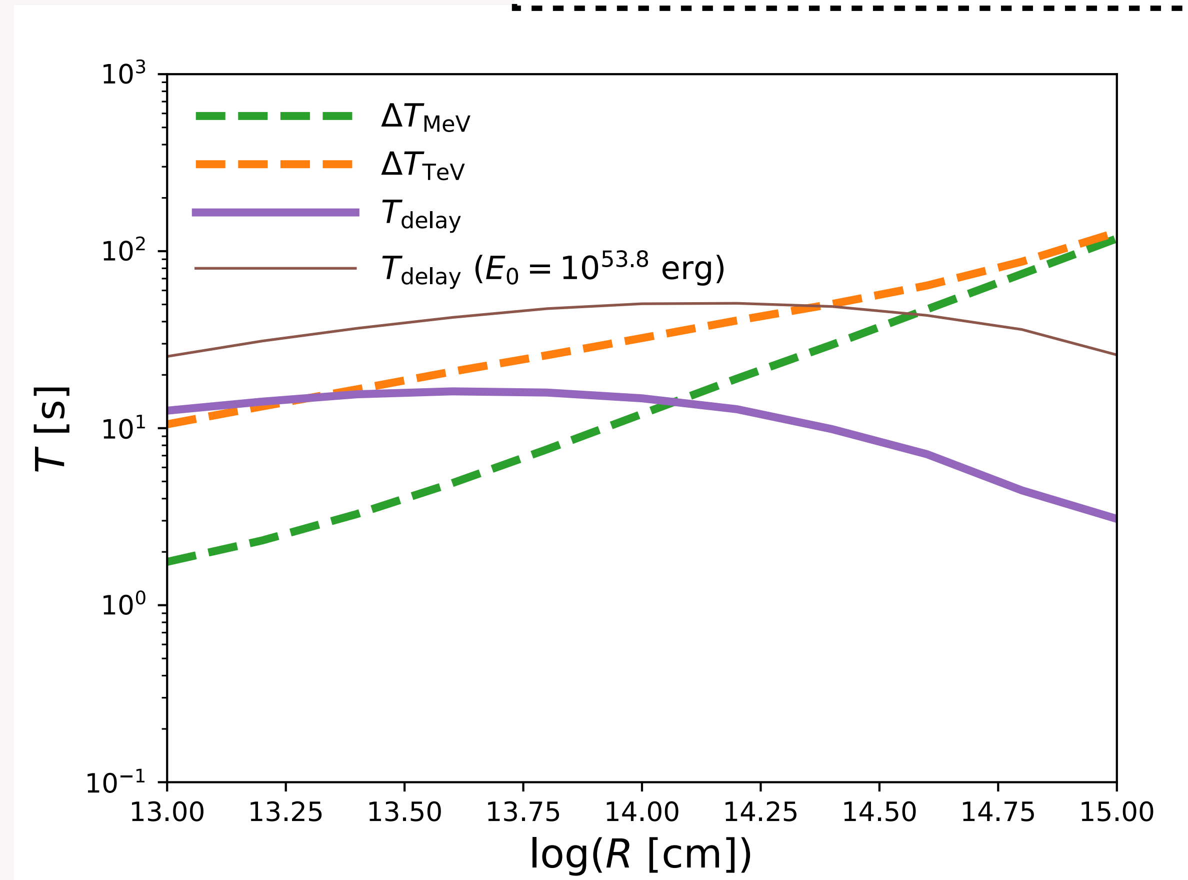

The typical arrival time of VHE photons could be delayed compared to the typical arrival time of prompt sub-MeV/MeV photons!

Summary - II

When considering the off-axis structured jets, we found that different enegry photons could arrive from different emission zones, mainly due to the effect of the two-photon pair annihilation process.

The main reason is that the optical depth for VHE photons is much higher in the core region on the jet surface, which gradually decreases outwards allowing VHE photons to escape.

The optical depth for VHE photons is sensitive to the emission radius, where the corresponding time delay between the typical arrival time of the TeV and MeV emission decreases with the increase of the emission radius.

Radiative models

Daigne, Bosnjak, Dubus 2011
Beniamini & Piran 2013

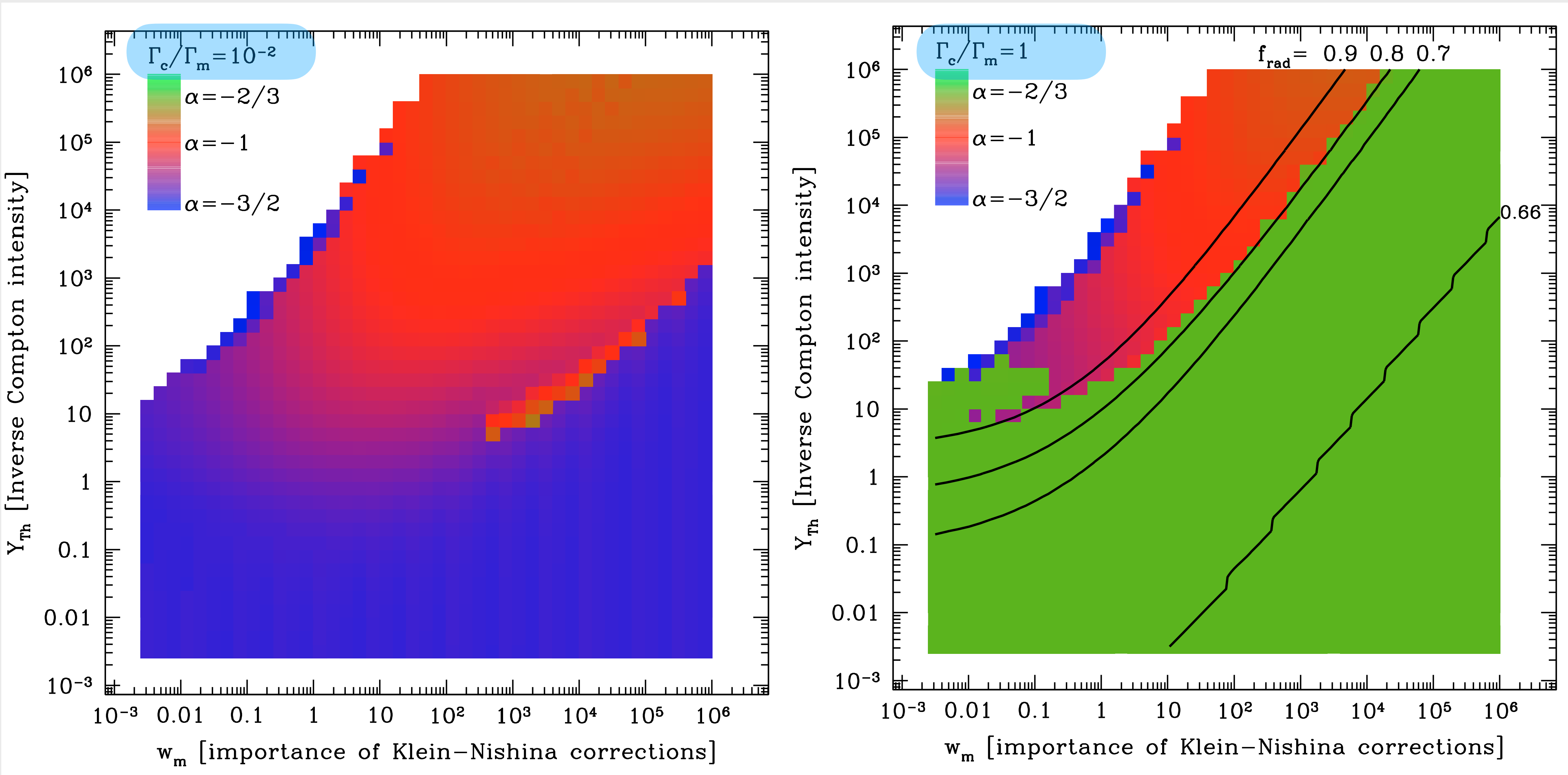

- "Marginally fast cooling regime": electrons are in fast cooling regime but not deeply in this regime, i.e. $\Gamma_c \lesssim \Gamma_m$ rather than $\Gamma_c \ll \Gamma_m$
- A large radiative efficiency (> 66%) can be achieved even for $\Gamma_c / \Gamma_m \simeq 1$

TeV observations: GRB 221009A

First GRB seen by an extensive air shower detector
(LHAASO collaboration, Science 2023)

TeV light curve: a rise to peak after a quiescent phase, then a decay

$E_{iso} \sim 10^{55}$ erg   z = 0.151

First time detection of the afterglow onset?

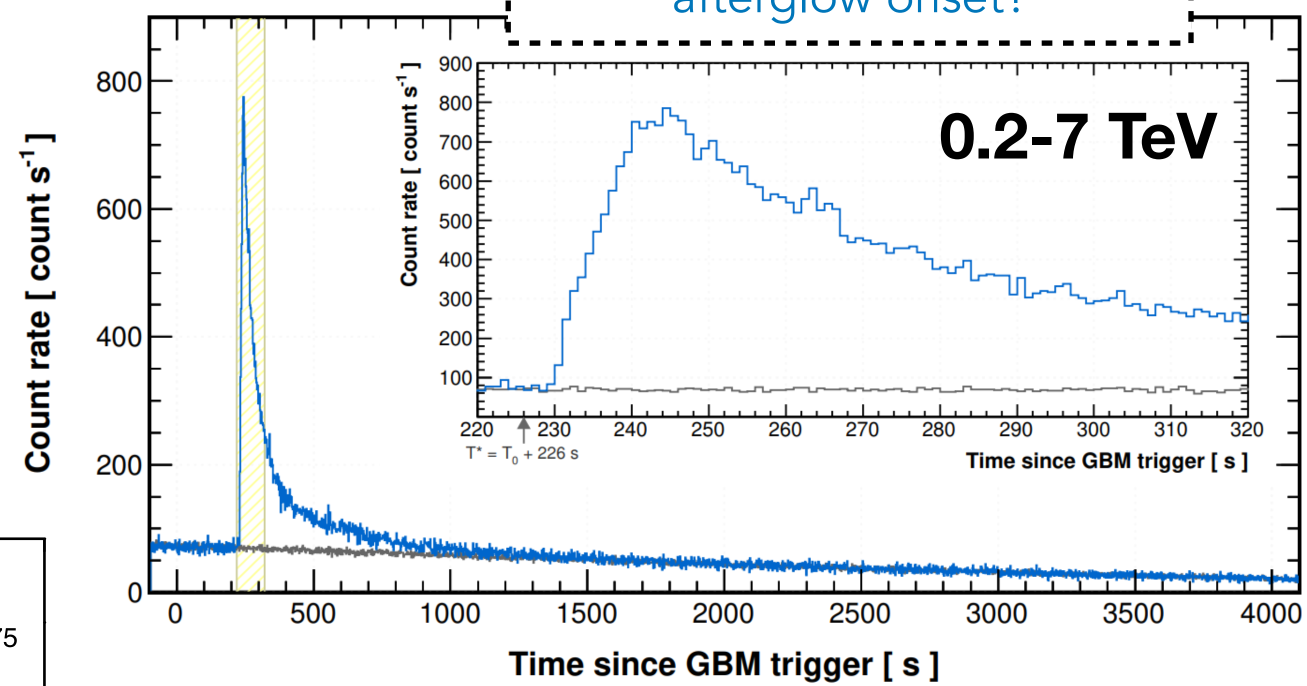

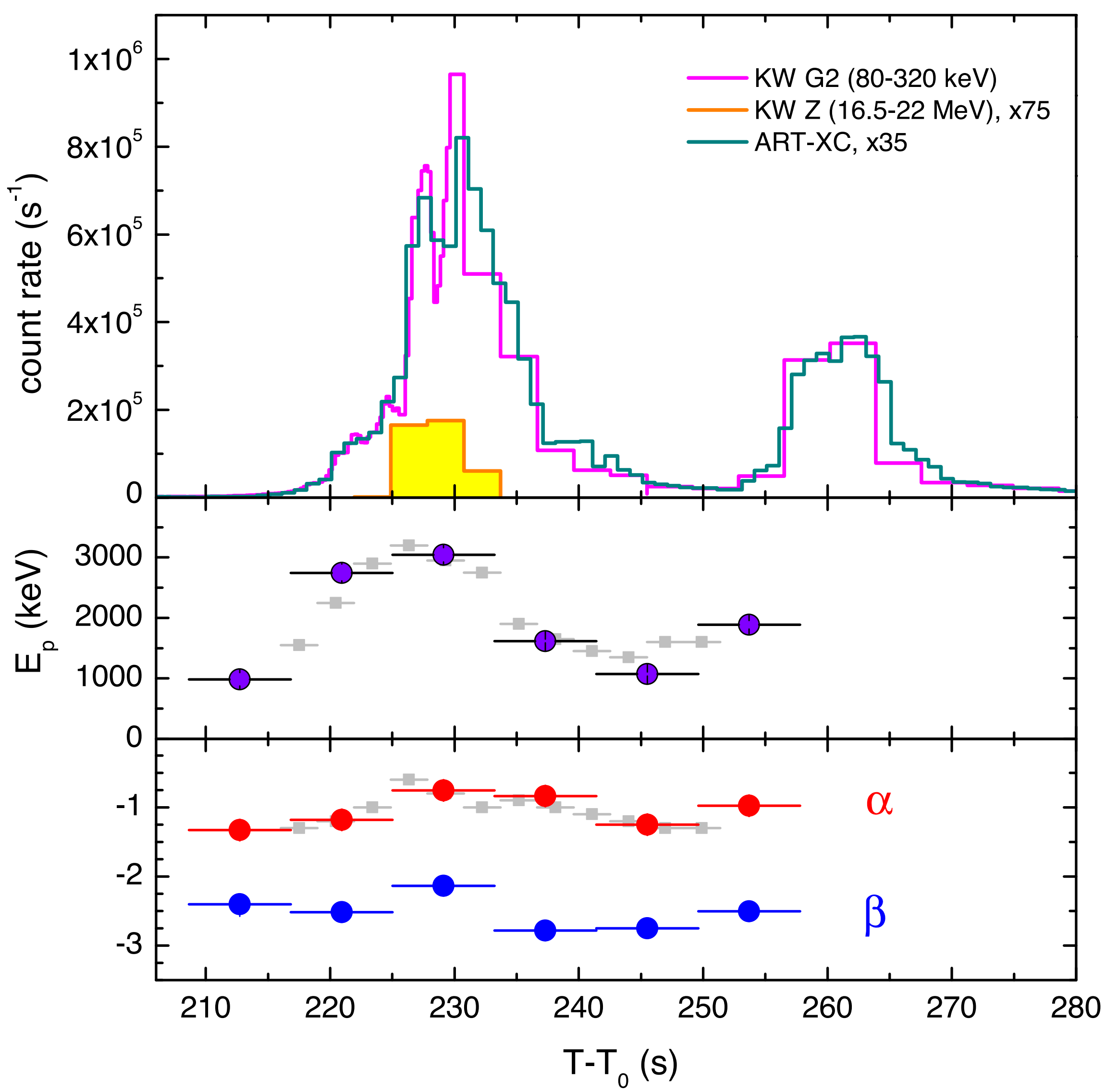

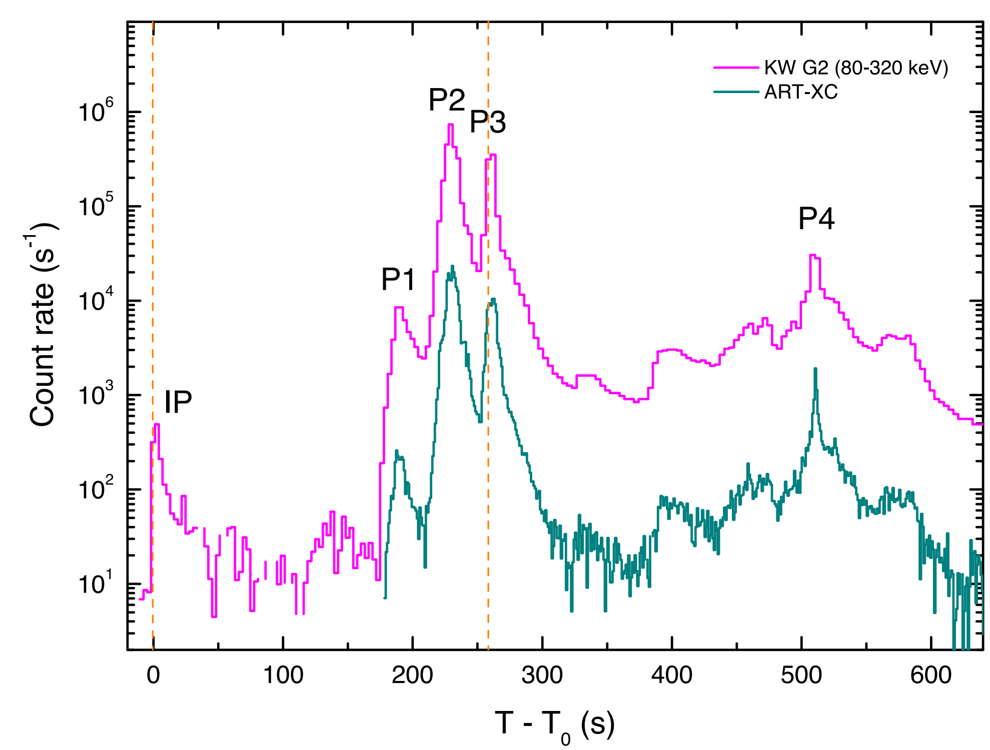

Frederiks et al. 2023: Konus-WIND and ART-XC (4- 30 keV) observations

X-ray afterglow of TeV/GeV events

Zhang et al. 2006

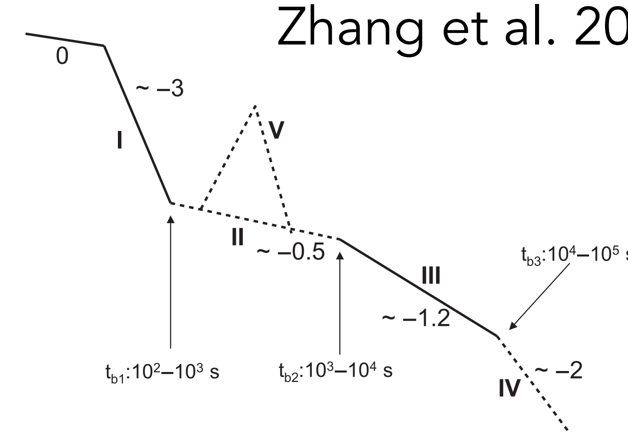

0 prompt
I steep decay
II shallow decay
III normal decay
IV post jet break
V flares

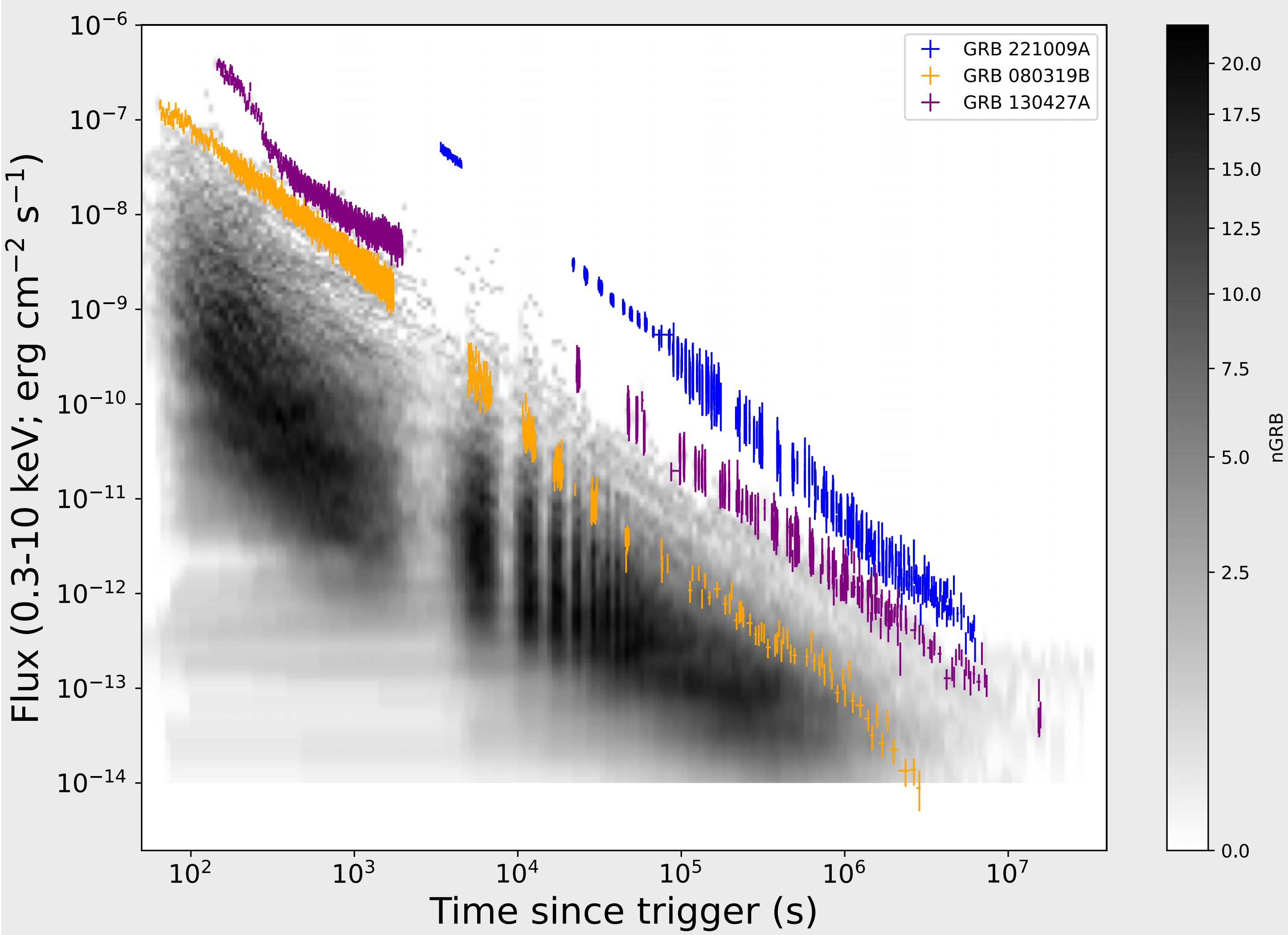

Observer frame 0.3-10 keV observed flux light curves: a comparison of GRB 221009A with all of GRBs observed by XRT (Williams, M. et al. 2023)

Early X_ray aferglow light curves of 26 events triggered by *Swift* BAT and detected by *Fermi* LAT and/or IACTs:

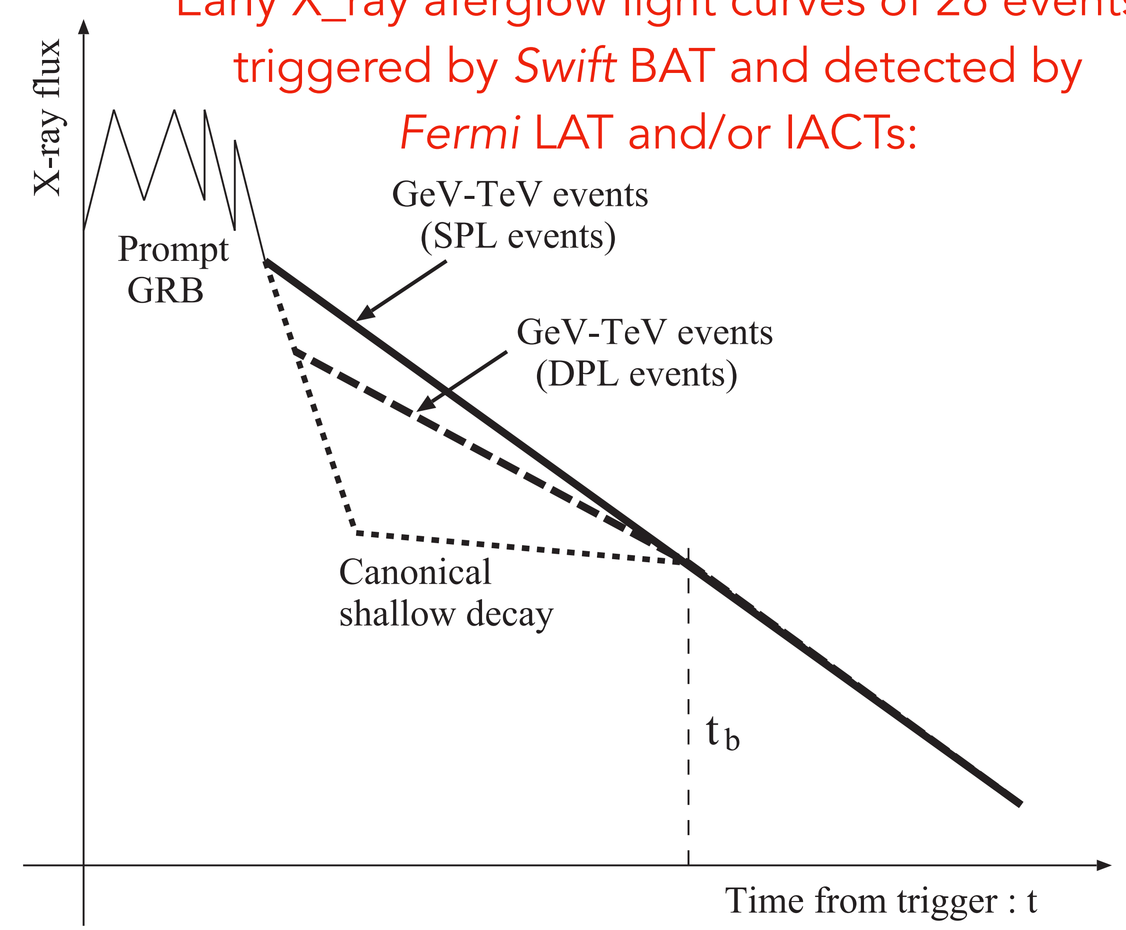

For the GeV/TeV bursts the fraction of events whose X-ray afterglows are described by single power law is significantly larger than those for non-GeV/TeV GRBs (Yamazaki, R. et al. 2020)

TeV observations: decaying afterglows?

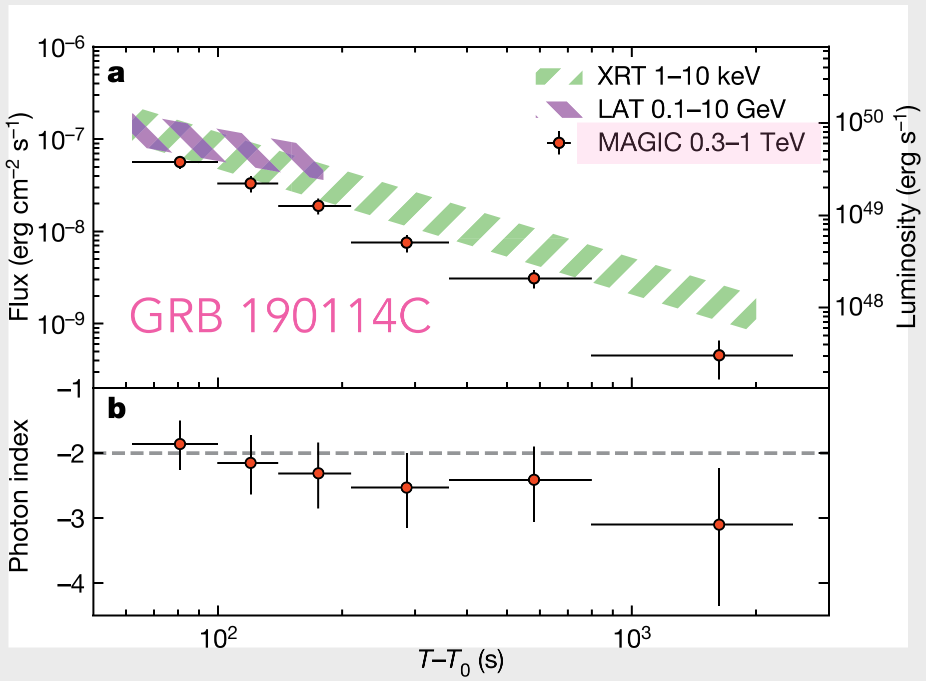

MAGIC collaboration 2019, Nature

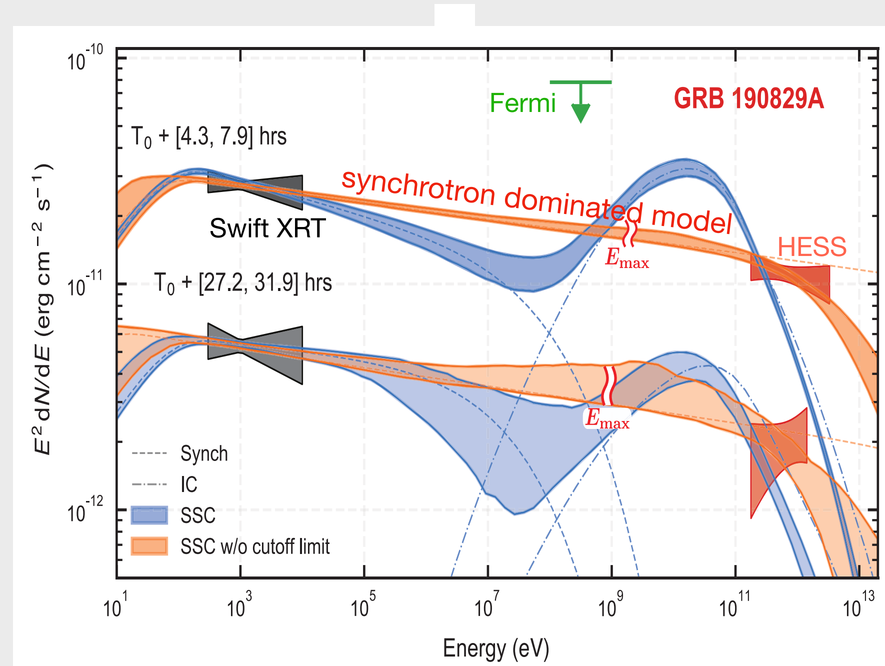

H.E.S.S. collaboration 2021, Science

GRB 160821B

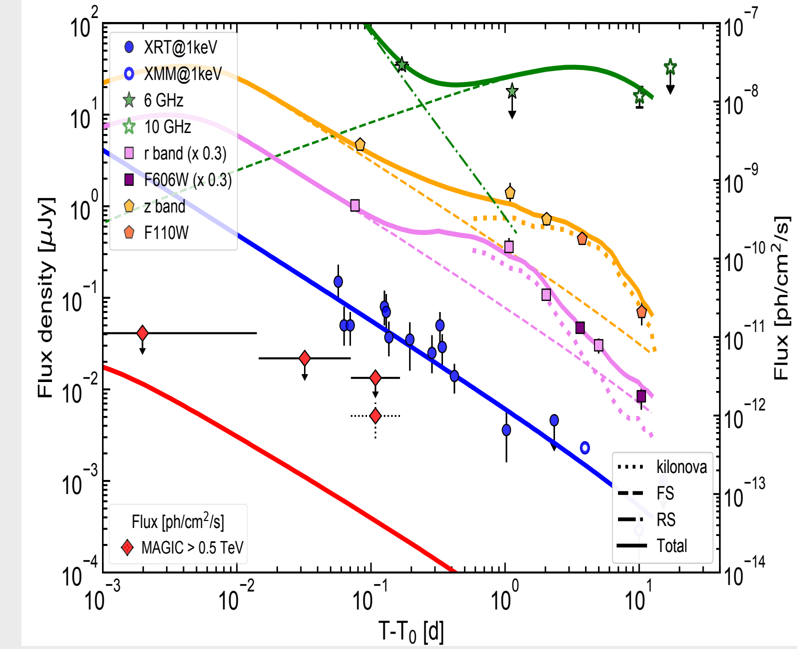

MAGIC collaboration, ApJ, 2021

MAGIC slew to the direction of GRB 190114C (z=0.42) about 50 s after the trigger and detected > 0.2 TeV photons

$E_{iso} \approx 3 \times 10^{53}$ erg

GRB 190829A: power law spectrum in the range (0.18-3.3) TeV $\gamma^{\rm int}_{\rm VHE}=2.07$

-low-luminosity GRB

-observed between 4 and 56 h after the trigger

z = 0.0785

$E_{iso} \approx 3 \times 10^{50}$ ergs

short GRB at z = 0.162

MAGIC observations started from 24 s after the trigger

Evidence of a gamma-ray signal above ~0.5 TeV until 4h after the burst

$E_{iso} \approx 1.2 \times 10^{49}$ erg

Distance measurements to dust clouds using GRB X-ray halos

- **Motivation**

Soft X-rays (~ few keV) are efficitenly scattered at small angles (θ ~ a few arcmin) by interstellar dust

Predicted by Overbeck (1965) and first time observed by Einstein Observatory (Rolf 1993; Catura 1983), due to dust scattering, point X-ray sources are surrounded by diffuse emission → X-ray dust halos

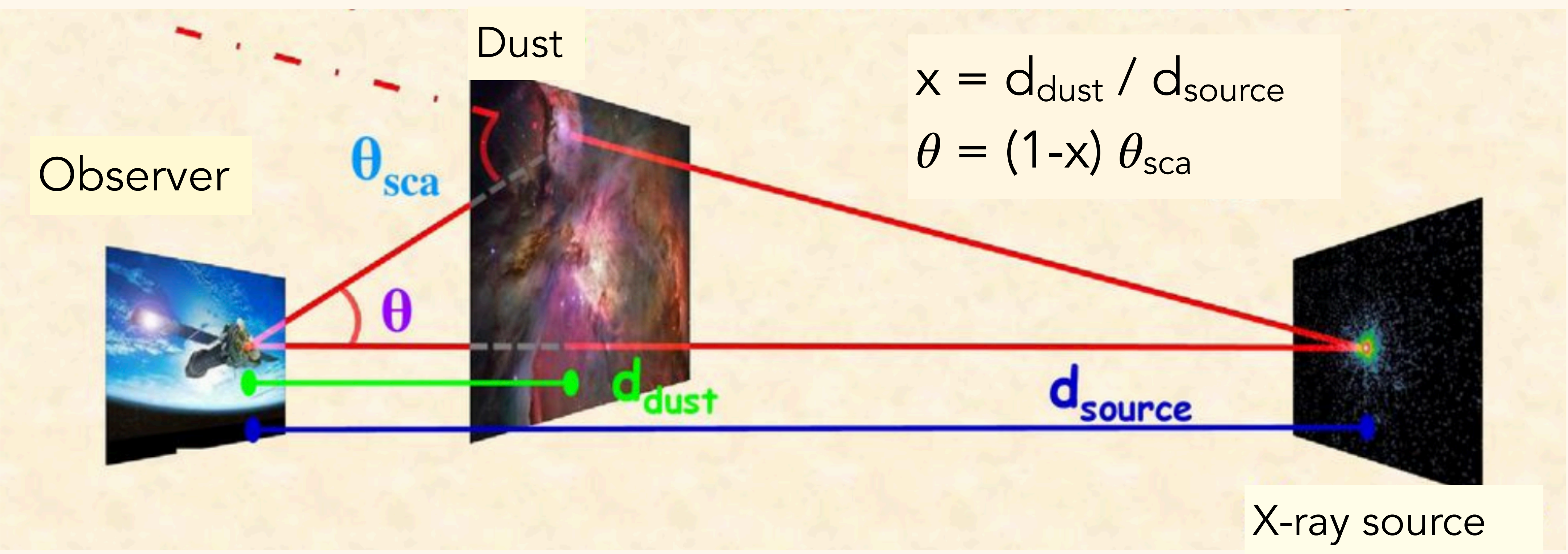

A. Tiengo

Distance measurements to dust clouds using GRB X-ray halos

- **Motivation**

Dust scattered X-rays detected at off-axis angle θ ($\approx \theta_{sca}$ if $d_{dust} << d_{source}$) will have a time delay:

$$t - t_0 = \frac{x}{1-x}\frac{d_{source}\theta^2}{2c}$$

$$\theta(t) = \sqrt{\frac{1-x}{x}\frac{2c(t-t_0)}{d_{source}}} \approx \sqrt{\frac{2c(t-t_0)}{d_{dust}}}$$ if $d_{dust} << d_{source}$

Halo photons scattered at larger radii suffer greater time delay owing to their longer paths.

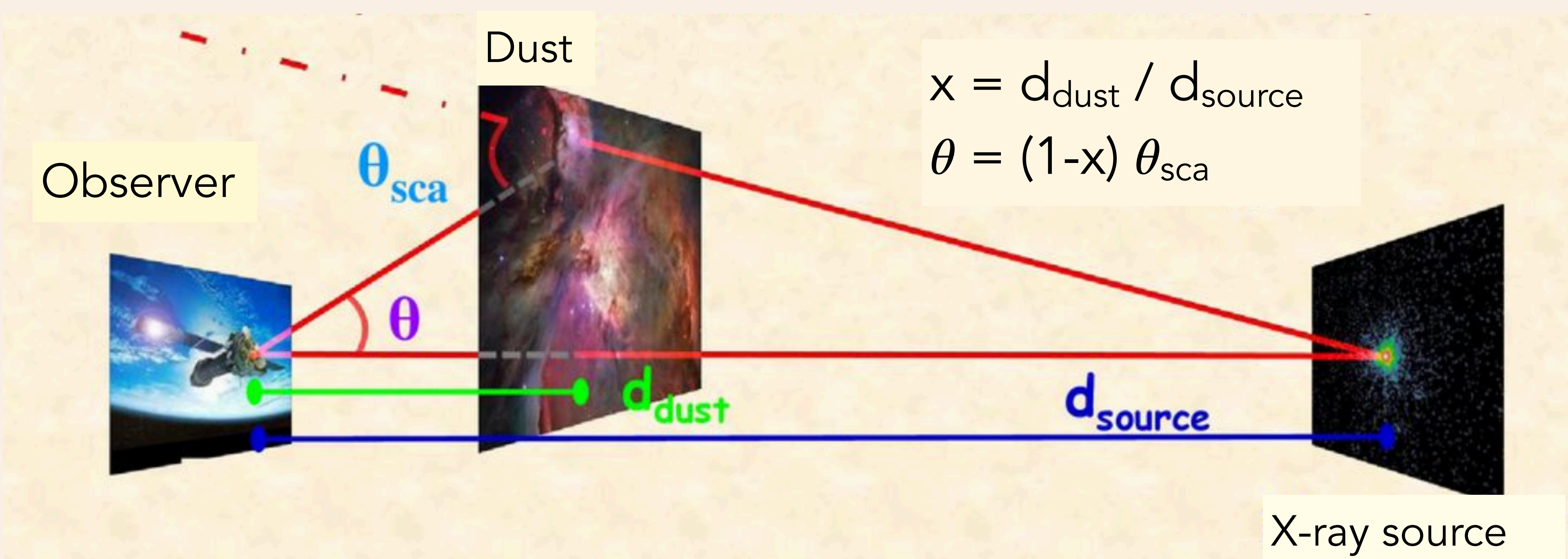

A. Tiengo

- **Dust-scattered X-ray halos around gamma-ray bursts**

If the halo surface brightness is sufficiently high, the expanding ring can be easily detected by comparing X-ray images taken at different times.

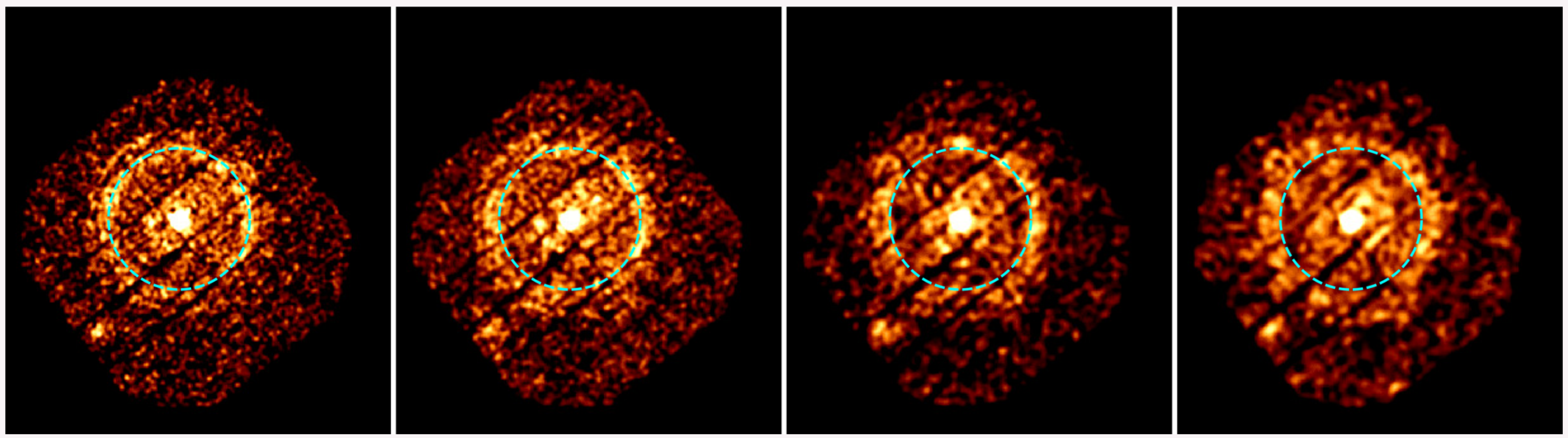

Pintore 2017: EPIC pn images in (1-2) keV, integrated for consecutive intervals of 14ks

Alternatively (Tiengo et al. 2006; Pintore et al. 2017), to visualise and detect an expanding X-ray ring, cosntructed **a dynamical image**: each count, detected with position x_i, y_i and arrival time T_i is binned according to

$$t_i = T_i - T_0$$
$$\theta_i^2 = (x_i - X_{\rm GRB})^2 + (y_i - Y_{\rm GRB})^2$$

$$D_i = 2ct_i/\theta_i^2 = 827 t_i[\mathrm{s}]/\theta_i^2[\mathrm{arcsec}]\ \mathrm{pc}$$

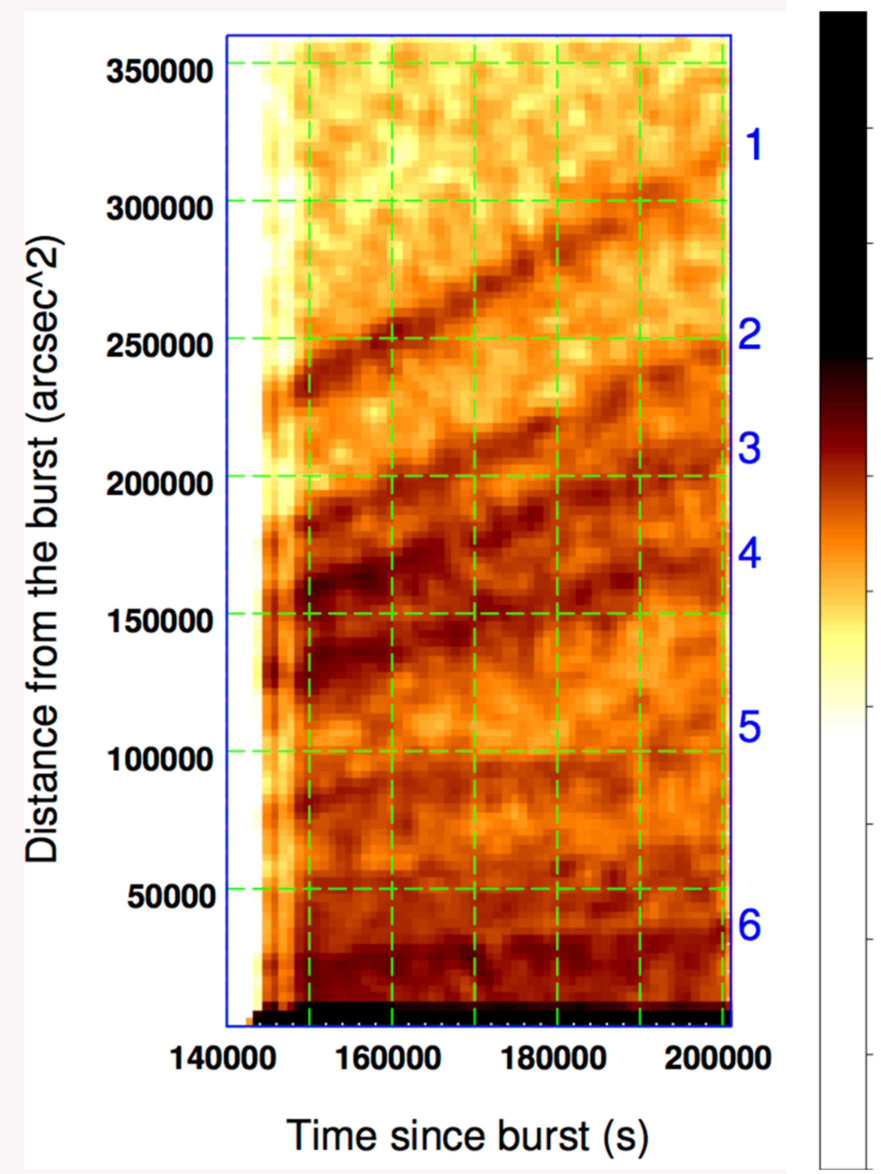

- **Comparison of distance measurements to dust clouds using GRB x-ray halos and 3D dust extinction**

We used four 3D extinction maps that exploit photometric data from different surveys and apply diverse algorithms for the 3D mapping of extinction and compared the X-ray halo derived distances with the local maxima in the 3D extinction density distribution.

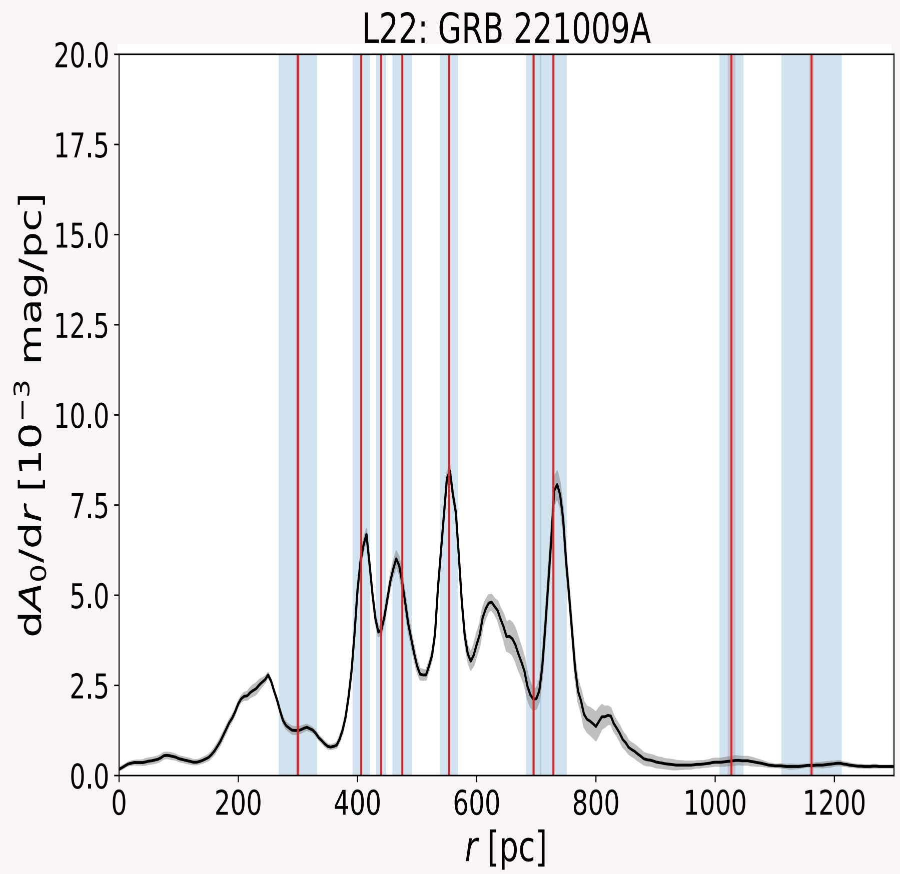

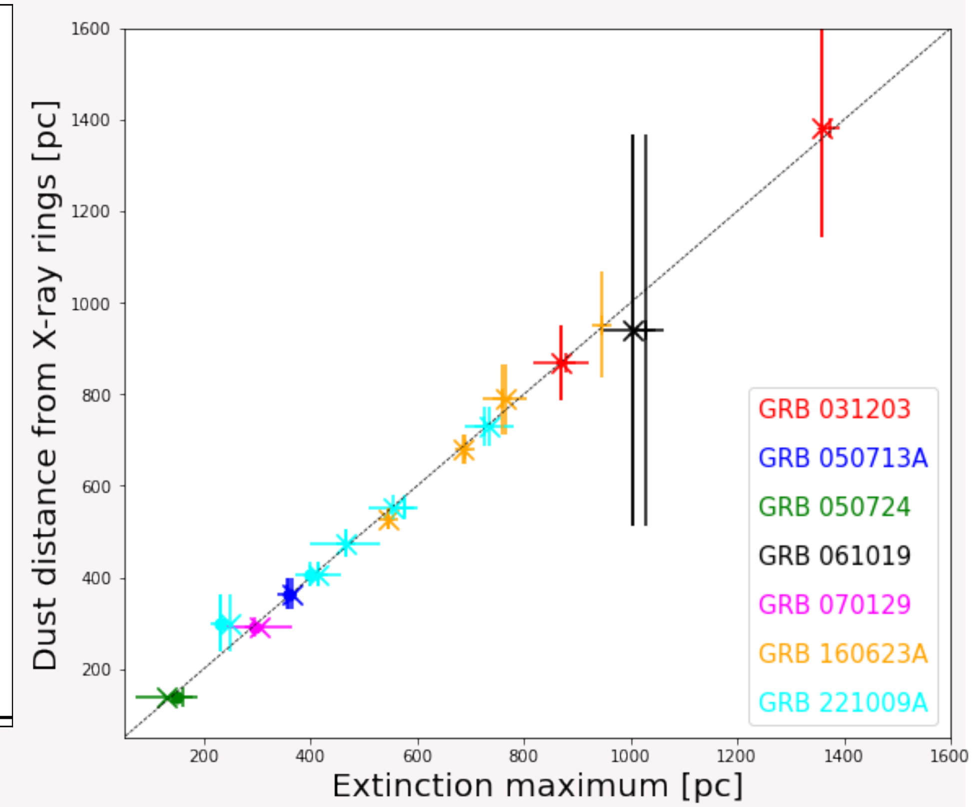

2D cut of extinction density cube from L22 map perpendicular to the plane of the galaxy in the direction of GRB 221009A. Height is measured with respect to the position of the plane of galaxy:

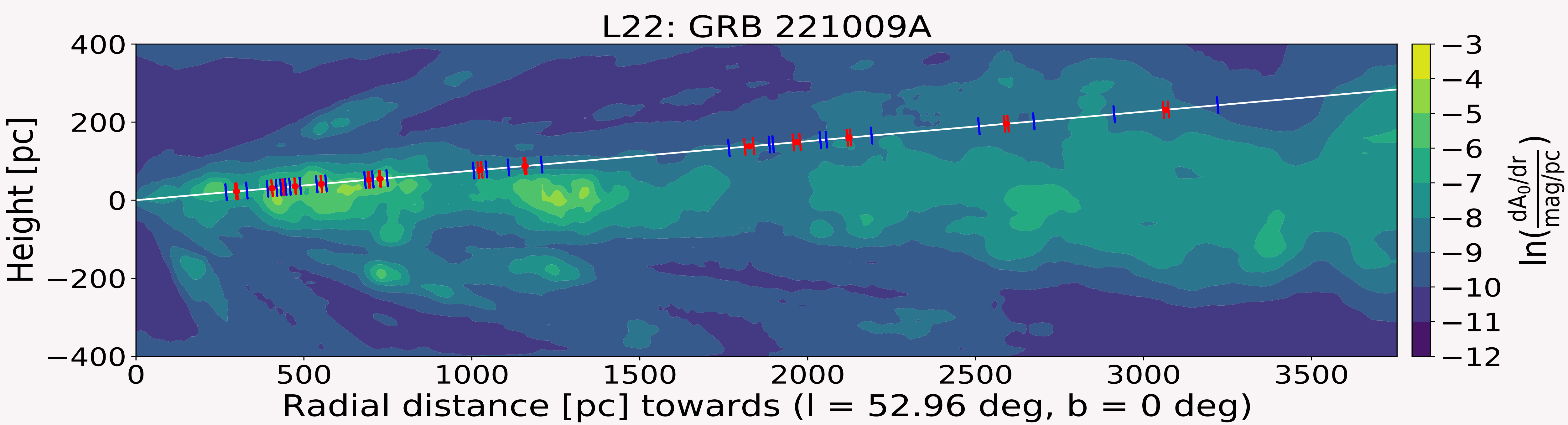

Šiljeg, ŽB, Tiengo et al. MNRAS 2023